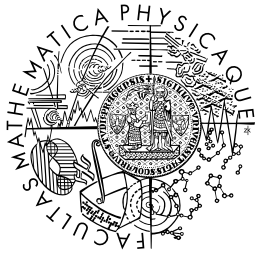

FACULTY
OF MATHEMATICS
AND PHYSICS
Charles University

BACHELOR THESIS

Tomáš Tuleja

Bootstrapping quantum mechanics and matrix models

Institute of Particle and Nuclear Physics

Supervisor of the bachelor thesis: Mgr. Petr Vaško, Ph.D.
Study programme: Physics
Study branch: FP Physics

Prague 2024

I declare that I carried out this bachelor thesis independently, and only with the cited sources, literature and other professional sources. It has not been used to obtain another or the same degree.

I understand that my work relates to the rights and obligations under the Act No. 121/2000 Sb., the Copyright Act, as amended, in particular the fact that the Charles University has the right to conclude a license agreement on the use of this work as a school work pursuant to Section 60 subsection 1 of the Copyright Act.

In ..... date ....

Author's signature

I want to thank my supervisor, Petr Vaško, for all our sessions, his guidance, and his willingness to explain many things to me. I learned a lot and really enjoyed it. I also thank my family for their support and my friends, who discussed new physical and mathematical concepts with me. In particular, I want to thank my beloved Elenka, who stood by my side the whole time.

Title: Bootstrapping quantum mechanics and matrix models

Author: Tomáš Tuleja

Institute: Institute of Particle and Nuclear Physics

Supervisor: Mgr. Petr Vaško, Ph.D., Institute of Particle and Nuclear Physics

Abstract: The conformal bootstrap is a numerical method used initially in Conformal Field Theory (CFT), which leverages symmetries and consistency conditions. We introduce the bootstrap ideas in quantum mechanics and test them in two simple models – the harmonic oscillator and the double-well. We estimate the spectrum of the harmonic oscillator and compare it to the well-known exact spectrum that can be found analytically. We also estimate the spectrum of the double-well potential and focus on the splitting of the ground state and the first excited state. We compare our estimate for ground-state splitting with the WKB approximation and path integral around instanton (one-loop approximation). These methods are not trivial; we describe them in great detail. The aim of this thesis is to introduce and test the bootstrap method on two simple quantum mechanical systems mentioned earlier using our implementation in Python and compare the obtained results with the results obtained analytically.

Keywords: Bootstrap, WKB approximation, Path integral, Instanton, One-loop approximation

Contents

Introduction

The conformal bootstrap is a numerical method used initially in Conformal Field Theory (CFT) leveraging symmetries and consistency conditions. It was used with great success in estimating the 3d Ising model critical exponents and could be used in attacking other very hard and famous models, such as the Banks-Fischler-Shenker-Susskind matrix model of quantum mechanics (BFSS). Han, Hartnoll, and Kruthoff [1] were the first to use the method on toy models in quantum mechanics and showed that it can be used to constrain or solve complicated systems that are not solvable by analytical approaches.

We introduce the bootstrap ideas in quantum mechanics and test them in two simple models – the harmonic oscillator and the double-well. We go through the details of implementing the bootstrapping algorithm in Python. We estimate the spectrum of the harmonic oscillator and compare it to the well-known exact spectrum that can be found analytically. We also estimate the spectrum of the double-well potential and focus on the splitting of the ground state and the first excited state. We compare our estimate for ground-state splitting with various approximation techniques.

We need to describe these approximation techniques in great detail since they are not trivial. Additionally, the applicability of these methods and concepts goes beyond the double-well potential. We start with the WKB approximation, a useful method for approximately solving the time-independent Schrödinger equation. We derive the method and use it to calculate ground-state energy splitting in the double-well potential. Then, we move on to a different approach using path integrals and their approximate calculation. We introduce the instanton and how the path integral around instanton can be used to calculate the ground-state energy splitting.

We assume the reader is familiar with calculus, complex analysis, linear algebra, quantum mechanics, and Python. All theory needed is derived along the way. It is the beginner's text on the bootstrap method. Therefore, we try to explain pedagogically by providing many computational details. We hope that the reader finds this more helpful than exhausting.

The aim of this thesis is to introduce and test the bootstrap method on two simple quantum mechanical systems mentioned earlier using our implementation and compare the obtained results with the results obtained analytically.

1. Theory

This chapter discusses two different theoretical methods to calculate the splitting of the ground state energy in the double-well potential. We will do the same thing in both methods because they give us the same result, but the approaches are very different. The first method focuses on the approximate solution of the time-independent Schrödinger equation. On the other hand, the second method uses the formalism of path integrals and their approximate calculation. Our use of these methods will concern the double-well potential. However, the applicability of both methods is wide-ranging. The first method is often used to describe tunneling through a given potential barrier or to obtain approximate solutions of time-independent Schrödinger equation for a given potential. The second method gives us a glimpse of the usage of path integrals in quantum mechanics, which is a perfect playground for introducing the topic before meeting them in more advanced field theories.

1.1 WKB approximation

We will examine the intricacies of the approximation technique for a particular class of differential equations. It is called WKB, and it is very useful in quantum mechanics. For a particle in a given potential, it will provide an ansatz for its wavefunction in classically allowed and forbidden regions. We will discuss the regions of validity of the approximation and how to connect WKB ansatzes from different regions of validity. We will have to dive into expansions of the Airy functions to tell how to connect correctly. Finally, we will apply this approximation to calculate the ground-state energy splitting of the double-well potential. We will follow the steps of [2], an alternative approach to the WKB through the Hamilton-Jacobi equation can be found in [3].

1.1.1 Approximation method

The WKB (Wentzel-Kramers-Brillouin) approximation technique provides approximate solutions for linear differential equations with slowly varying coefficients. What is meant by slowly is part of one of the sections ahead. In the context of quantum mechanics, we call it also a semiclassical approximation since we will work formally with $\hbar$ as a small expansion parameter, and insights from classical mechanics will help us understand the form of the wavefunction. The linear differential equation in question will be a time-independent Schrödinger equation.

Suppose we have a particle of mass m and total energy E, in potential $V(x)$. We will define the local momentum of the particle

$$p^2(x) \equiv 2m(E - V(x)), \tag{1.1}$$

and local de Broglie wavelength

$$\lambda(x) \equiv \frac{2\pi\hbar}{p(x)}. \tag{1.2}$$

Time-independent Schrödinger equation can be rewritten in terms of local momentum and momentum operator

$$-\frac{\hbar^2}{2m}\frac{\mathrm{d}^2}{\mathrm{d}x^2}\psi(x) = (E - V(x))\psi(x),$$
$$\hat{p}^2\psi(x) = p^2(x)\psi(x). \tag{1.3}$$

The equation above looks like an eigenvalue equation, but it is not one; $p^2(x)$ is a function of position.

Our goal is to find approximative solutions for the wavefunction $\psi(x)$, which is a solution of the time-independent Schrödinger equation. In the case of a constant potential, the solutions become plane waves

$$\psi(x) \sim \exp\left(\frac{i}{\hbar}px\right). \tag{1.4}$$

We expect that the slowly varying potential will affect only the exponent. Because of that, we will use an ansatz for solution in the form

$$\psi(x) = \exp\left(\frac{i}{\hbar}S(x)\right),\ S(x) \in \mathbb{C}. \tag{1.5}$$

We will plug this ansatz into equation (1.3), we get

$$-\hbar^2\frac{\mathrm{d}^2}{\mathrm{d}x^2}\exp\left(\frac{i}{\hbar}S(x)\right) = p^2(x)\exp\left(\frac{i}{\hbar}S(x)\right),$$
$$-\hbar^2\left[\frac{i}{\hbar}S''(x) - \frac{(S'(x))^2}{\hbar^2}\right]\exp\left(\frac{i}{\hbar}S(x)\right) = p^2(x)\exp\left(\frac{i}{\hbar}S(x)\right),$$
$$(S'(x))^2 - i\hbar S''(x) = p^2(x). \tag{1.6}$$

We will argue that $\hbar S''(x)$ is small for slowly varying potentials. If we have constant potential $V(x) = V_0$, then $p(x) = p_0$ and $S'(x) = p_0$ is a solution to equation (1.6). Therefore, $S''(x) = 0$, and we expect that $S''(x)$ will be small for the slowly varying potential. Since we work in the limit $\hbar \to 0$, term $\hbar S''(x)$ is small indeed. We will expand $S(x)$ in powers of $\hbar$

$$S(x) = S_0(x) + \hbar S_1(x) + \hbar^2 S_2(x) + \mathcal{O}(\hbar^3), \tag{1.7}$$

and use it in equation (1.6) to obtain

$$(S_0' + \hbar S_1' + \hbar^2 S_2' + ...)^2 - i\hbar(S_0'' + \hbar S_1'' + \hbar^2 S_2'' + ...) - p^2 = 0,$$
$$(S_0')^2 - p^2 + \hbar(2S_0'S_1' - iS_0'') + \mathcal{O}(\hbar^2) = 0. \tag{1.8}$$

We get two separate equations

$$(S_0')^2 - p^2 = 0, \tag{1.9}$$
$$2S_0'S_1' - iS_0'' = 0. \tag{1.10}$$

From equation (1.9) and (1.10) we see that

$$S_0' = \pm p \quad \Rightarrow \quad S_0(x) = \pm\int_{x_0}^{x} p(x')\,\mathrm{d}x',\ x_0 < x, \tag{1.11}$$
$$S_1' = \frac{i}{2}\frac{S_0''}{S_0'} = \frac{i}{2}\frac{p'}{p} \quad \Rightarrow \quad iS_1(x) = -\frac{1}{2}\ln p(x) + C,\ C \in \mathbb{C}, \tag{1.12}$$

where x_0 and C are the constants of integration. Looking back at our ansatz for the wavefunction (1.5), we have

$$\begin{aligned}\psi(x) &= \exp\left[\frac{i}{\hbar}(S_0(x) + \hbar S_1(x) + \mathcal{O}(\hbar^2))\right] \simeq \\ &\simeq \exp\left(\frac{i}{\hbar}S_0(x)\right)\exp(iS_1(x)) = \\ &= \exp\left(\pm\frac{i}{\hbar}\int_{x_0}^{x} p(x')\,\mathrm{d}x'\right)\exp\left(-\frac{1}{2}\ln p(x) + C\right) = \\ &= \frac{A}{\sqrt{p(x)}}\exp\left(\pm\frac{i}{\hbar}\int_{x_0}^{x} p(x')\,\mathrm{d}x'\right), \end{aligned} \tag{1.13}$$

from which we get a so-called basic solution in the WKB approximation

$$\psi(x) \simeq \frac{A}{\sqrt{p(x)}}\exp\left(\pm\frac{i}{\hbar}\int_{x_0}^{x} p(x')\,\mathrm{d}x'\right),\ A \in \mathbb{C}. \tag{1.14}$$

Let us present two implications of this result.

1. Calculation of probability density gives us

$$\rho(x) = \psi^*(x)\psi(x) = \frac{|A|^2}{p(x)} = \frac{|A|^2}{mv(x)}, \tag{1.15}$$

   where $v(x)$ is the local velocity of the particle. For small values of $v(x)$, we get big values of $\rho(x)$. In other words, it is more probable to find the particle in places where it is slower, which is a result we would expect.

2. Calculation of probability current gives us

$$J(x) = \frac{\hbar}{m}\mathrm{Im}(\psi^*(x)\psi'(x)) = \rho(x)\frac{\pm p(x)}{m} = \pm\frac{|A|^2}{p(x)}\frac{p(x)}{m} = \pm\frac{|A|^2}{m}. \tag{1.16}$$

   It should not be surprising to find that the probability current is constant. The continuity equation tells us

$$\frac{\partial\rho}{\partial t} + \frac{\partial J}{\partial x} = 0, \tag{1.17}$$

   but probability density is time-independent in our case, and we get

$$\frac{\partial\rho}{\partial t} = 0 \quad\Rightarrow\quad J(x) = \text{const}. \tag{1.18}$$

We will apply the basic solution in WKB approximation to areas deep in classically allowed and forbidden regions. For classically allowed region is $E - V(x) > 0$ and we will denote $p^2(x) = \hbar^2 k^2(x)$, $k(x) > 0$. Then equation (1.3) has the form

$$\psi''(x) = -k^2(x)\psi(x), \tag{1.19}$$

and the basic solution is

$$\psi(x) = \frac{A}{\sqrt{k(x)}}\exp\left(-i\int_{x_0}^{x} k(x')\,\mathrm{d}x'\right) + \frac{B}{\sqrt{k(x)}}\exp\left(i\int_{x_0}^{x} k(x')\,\mathrm{d}x'\right). \tag{1.20}$$

For classically forbidden region is $E - V(x) < 0$ and we will denote $p^2(x) = -\hbar^2\kappa^2(x)$, $\kappa(x) > 0$. Then equation (1.3) has the form

$$\psi''(x) = \kappa^2(x)\psi(x), \tag{1.21}$$

and the basic solution is

$$\psi(x) = \frac{C}{\sqrt{\kappa(x)}} \exp\left(-\int_{x_0}^{x} \kappa(x')\,\mathrm{d}x'\right) + \frac{D}{\sqrt{\kappa(x)}} \exp\left(\int_{x_0}^{x} \kappa(x')\,\mathrm{d}x'\right). \tag{1.22}$$

1.1.2 Validity of the approximation

We will specify the meaning of slowly varying potential and establish the region of validity of the basic solution (1.14). We will go back to the expansion in powers of $\hbar$

$$(S_0')^2 - p^2 + \hbar(2S_0'S_1' - iS_0'') + \mathcal{O}(\hbar^2) = 0. \tag{1.23}$$

The $\mathcal{O}(\hbar)$ terms must be lot less than $\mathcal{O}(1)$ terms. Because of equations (1.9) and (1.10) it is sufficient to compare one $\mathcal{O}(\hbar)$ term with one $\mathcal{O}(1)$ term, for example

$$|\hbar S_0'S_1'| \ll |S_0'|^2 \quad \Rightarrow \quad |\hbar S_1'| \ll |p|. \tag{1.24}$$

We know from equation (1.12) that $S_1' \sim |p'/p|$. Therefore

$$\hbar\left|\frac{p'}{p}\right| \ll |p|. \tag{1.25}$$

There are three ways to interpret this result.

- Changes in the local momentum over a distance of de Broglie wavelength λ are small compared to the momentum

$$\left|\frac{\hbar}{p}\right| |p'| \ll |p| \quad \Rightarrow \quad \lambda|p'| \ll |p|. \tag{1.26}$$

- The local de Broglie wavelength $\lambda(x)$ must vary slowly

$$\left|\hbar\frac{p'}{p^2}\right| \ll 1 \quad \Rightarrow \quad \left|\hbar\left(\frac{1}{p}\right)'\right| \ll 1 \quad \Rightarrow \quad |\lambda'| \ll 1. \tag{1.27}$$

- Change in potential over a distance of de Broglie wavelength λ is small compared to kinetic energy

$$\begin{aligned} p^2 = 2m(E-V) \quad &\Rightarrow \quad |pp'| = m|V'|, \\ |\lambda V'| = \frac{2\pi\hbar}{m}|p'| \ll \frac{p^2}{m} \quad &\Rightarrow \quad |\lambda V'| \ll \frac{p^2}{2m}. \end{aligned} \tag{1.28}$$

  The equation above is what we mean by slowly changing potential.

Suppose we have a particle in a potential $V(x)$ depicted in Figure 1.1. The particle's total energy E is such that the turning point is at $x = a$ (turning points are points where $E = V(x)$). Near $x = a$, we can approximate the potential as a linear function

$$V(x) - E \simeq g(x - a),\ g > 0. \tag{1.29}$$

In the classically allowed region $x < a$, we have

$$\begin{aligned} p^2(x) &= 2m(E - V(x)) \simeq 2mg(a - x), \\ |\lambda(x)| &= \frac{2\pi\hbar}{|p(x)|} \simeq \frac{2\pi\hbar}{\sqrt{2mg}\sqrt{a-x}} \quad \Rightarrow \quad |\lambda'| \simeq \frac{\pi\hbar}{\sqrt{2mg}} \frac{1}{(a-x)^{\frac{3}{2}}}. \end{aligned} \tag{1.30}$$

We can see that the vicinity of the turning point is a problem. As $x \to a$, $|\lambda'| \to \infty$, which is violation of the validity condition (1.28). We need a connection formula connecting WKB solutions in classically allowed and forbidden regions.

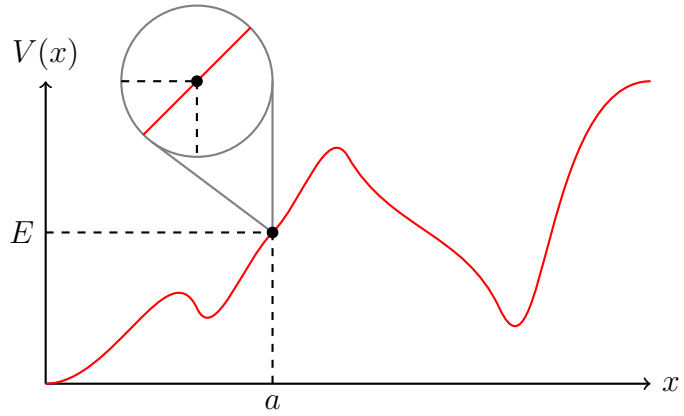

Figure 1.1: The potential $V(x)$ is approximately linear near the point (a,E).

1.1.3 Airy functions

The study of a linear potential is crucial for understanding behavior near the turning point. We will study a particle in the linear potential

$$V(x) = gx,\ x \in \mathbb{R},\ g > 0, \tag{1.31}$$

with total energy E such that turning point is located in $x = a$

$$V(x) - E = g(x - a). \tag{1.32}$$

Time-independent Schrödinger equation is in the form

$$-\frac{\hbar^2}{2m}\frac{\mathrm{d}^2\psi}{\mathrm{d}x^2} + g(x-a)\psi = 0. \tag{1.33}$$

To remove units from this equation, we introduce length parameter $L = \sqrt[3]{\frac{\hbar^2}{2mg}}$ and unit-free variable $u = \frac{1}{L}(x - a)$. We can rewrite (1.33) in terms of this new variable to get the Airy equation

$$\frac{\mathrm{d}^2\psi}{\mathrm{d}u^2} = u\psi. \tag{1.34}$$

Solutions to the equation above are not elementary functions but the Airy functions

$$\psi(u) = \mathrm{Ai}(u) = \mathrm{Ai}\left[\frac{1}{L}\left(x - \frac{E}{g}\right)\right]. \tag{1.35}$$

We will write WKB solutions for $u \ll -1$ and $u \gg 1$, deep in allowed and forbidden regions. Problems arise around $u = 0$, where the turning point is located. If we compare Airy equation (1.34) with equation (1.21) we see that for $u \gg 1$ and $\kappa \to \sqrt{u}$ we get

$$\begin{aligned}\psi(u) &= \frac{C}{u^{\frac{1}{4}}} \exp\left(-\int_{u_0}^{u} \sqrt{u'}\,\mathrm{d}u'\right) + \frac{D}{u^{\frac{1}{4}}} \exp\left(\int_{u_0}^{u} \sqrt{u'}\,\mathrm{d}u'\right) = \\ &= \frac{C}{u^{\frac{1}{4}}} \exp\left(-\frac{2}{3}u^{\frac{3}{2}}\right) + \frac{D}{u^{\frac{1}{4}}} \exp\left(\frac{2}{3}u^{\frac{3}{2}}\right),\end{aligned} \tag{1.36}$$

where the constant of integration $u_0 \in [0, u)$ was chosen for convenience to be zero (which is also the turning point). If we compare Airy equation (1.34) with equation (1.19) we see that for $u \ll -1$ and $k \to \sqrt{-u} = |u|^{\frac{1}{2}}$ we get

$$\begin{aligned}\psi(u) &= \frac{A}{|u|^{\frac{1}{4}}} \exp\left(i\int_{u}^{0} \sqrt{-u'}\,\mathrm{d}u'\right) + \frac{B}{|u|^{\frac{1}{4}}} \exp\left(-i\int_{u}^{0} \sqrt{-u'}\,\mathrm{d}u'\right) = \\ &= \frac{A}{|u|^{\frac{1}{4}}} \exp\left(i\frac{2}{3}|u|^{\frac{3}{2}}\right) + \frac{B}{|u|^{\frac{1}{4}}} \exp\left(-i\frac{2}{3}|u|^{\frac{3}{2}}\right).\end{aligned} \tag{1.37}$$

We could have used an alternative approach to solve the linear potential. The time-independent Schrödinger equation with linear potential is easily solvable in momentum representation. That way, we can go from the second-order to the first-order linear differential equation. The solution in coordinate representation can be written as a Fourier transformation

$$\psi(u) = \int_{-\infty}^{\infty} \frac{\mathrm{d}k}{2\pi}\, \widetilde{\psi}(k) e^{iku}, \tag{1.38}$$

where $\widetilde{\psi}(k)$ is a solution in momentum space and k is also unit-free. This way, we obtain only one linearly independent solution, but we know that the original coordinate representation is a second-order linear differential equation and must have two linearly independent solutions.

It will prove very convenient to analyze the Airy functions more closely, especially their asymptotic expansions. For more generality, instead of integrating over a full real line, we will integrate over some oriented contour Γ in complex k plane with starting point k_- and endpoint k_+ depicted in Figure 1.2

$$\psi(u) = \int_{\Gamma} \frac{\mathrm{d}k}{2\pi}\, \widetilde{\psi}(k) e^{iku}. \tag{1.39}$$

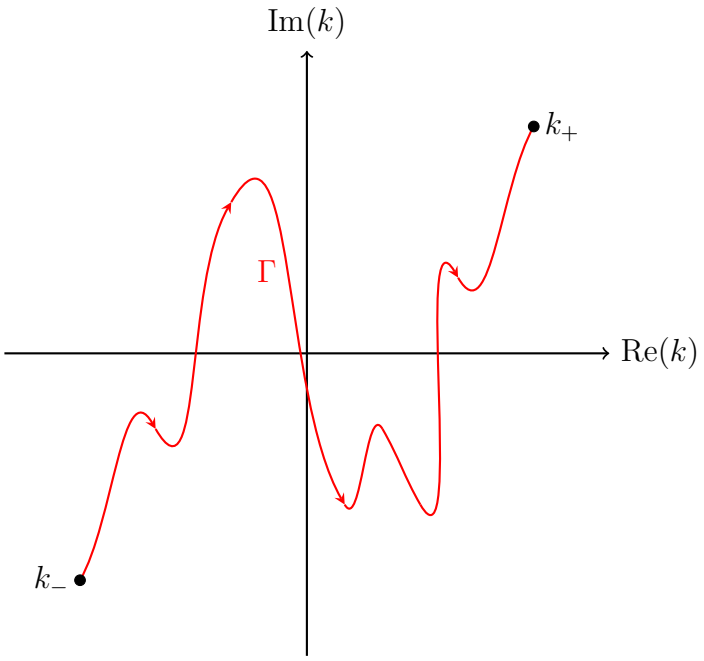

Figure 1.2: The oriented contour Γ in the complex k plane.

We will plug this ansatz into the Airy equation. Left-hand side gives

$$\frac{\mathrm{d}^2\psi}{\mathrm{d}u^2} = \frac{\mathrm{d}^2}{\mathrm{d}u^2}\int_\Gamma \frac{\mathrm{d}k}{2\pi}\,\widetilde{\psi}(k)e^{iku} = \int_\Gamma \frac{\mathrm{d}k}{2\pi}\,(-k^2\widetilde{\psi}(k))e^{iku}, \tag{1.40}$$

and the right-hand side gives

$$\begin{aligned} u\psi &= \int_\Gamma \frac{\mathrm{d}k}{2\pi}\,\widetilde{\psi}(k)ue^{iku} = \int_\Gamma \frac{\mathrm{d}k}{2\pi}\,\widetilde{\psi}(k)\frac{1}{i}\frac{\mathrm{d}}{\mathrm{d}k}(e^{iku}) = \\ &= \int_\Gamma \frac{\mathrm{d}k}{2\pi}\left[\frac{1}{i}\frac{\mathrm{d}}{\mathrm{d}k}(\widetilde{\psi}(k)e^{iku}) - \frac{1}{i}\frac{\mathrm{d}\widetilde{\psi}}{\mathrm{d}k}e^{iku}\right] = \\ &= \frac{1}{2\pi i}\left[\widetilde{\psi}(k)e^{iku}\right]_{k_-}^{k_+} - \int_\Gamma \frac{\mathrm{d}k}{2\pi}\,\frac{1}{i}\frac{\mathrm{d}\widetilde{\psi}}{\mathrm{d}k}e^{iku}. \end{aligned} \tag{1.41}$$

Putting it all together, we get

$$0 = \frac{\mathrm{d}^2\psi}{\mathrm{d}u^2} - u\psi = \int_\Gamma \frac{\mathrm{d}k}{2\pi}\left(-k^2\widetilde{\psi}(k) + \frac{1}{i}\frac{\mathrm{d}\widetilde{\psi}}{\mathrm{d}k}\right)e^{iku} - \frac{1}{2\pi i}\left[\widetilde{\psi}(k)e^{iku}\right]_{k_-}^{k_+}. \tag{1.42}$$

We have a solution if

$$-k^2\widetilde{\psi}(k) + \frac{1}{i}\frac{\mathrm{d}\widetilde{\psi}}{\mathrm{d}k} = 0, \tag{1.43}$$

$$\widetilde{\psi}(k_-)e^{ik_-u} = 0,\ \widetilde{\psi}(k_+)e^{ik_+u} = 0. \tag{1.44}$$

Boundary conditions in (1.44) tell us that terms must vanish separately. If they cancel each other out, we get a closed contour, which can be shrunk to zero size (because no poles are present), giving a trivial solution. Because we are looking for nontrivial solutions, terms in (1.44) must vanish separately. Solution to equation (1.43) is (up to normalization)

$$\widetilde{\psi}(k) = e^{\frac{ik^3}{3}}. \tag{1.45}$$

Thus, we have

$$\psi(u) = \int_\Gamma \frac{\mathrm{d}k}{2\pi} e^{\frac{ik^3}{3}} e^{iku}. \tag{1.46}$$

However, this is true only when boundary conditions (1.44) are met. After plugging (1.45) into (1.44), we get

$$e^{\frac{ik_-^3}{3}} e^{ik_- u} = e^{\frac{ik_+^3}{3}} e^{ik_+ u} = 0. \tag{1.47}$$

We are interested in asymptotic behavior $|k| \to \infty$, in that case the $e^{\frac{ik^3}{3}}$ term can vanish if $\mathrm{Im}(k^3) > 0$. If we write $k = |k|e^{i\theta_k}$ then

$$\begin{aligned} &\mathrm{Im}(k^3) = |k^3| \sin(3\theta_k) > 0 \\ &\theta_k \in \left[0, \frac{1}{3}\pi\right], \theta_k \in \left[\frac{2}{3}\pi, \pi\right], \theta_k \in \left[\frac{4}{3}\pi, \frac{5}{3}\pi\right]. \end{aligned} \tag{1.48}$$

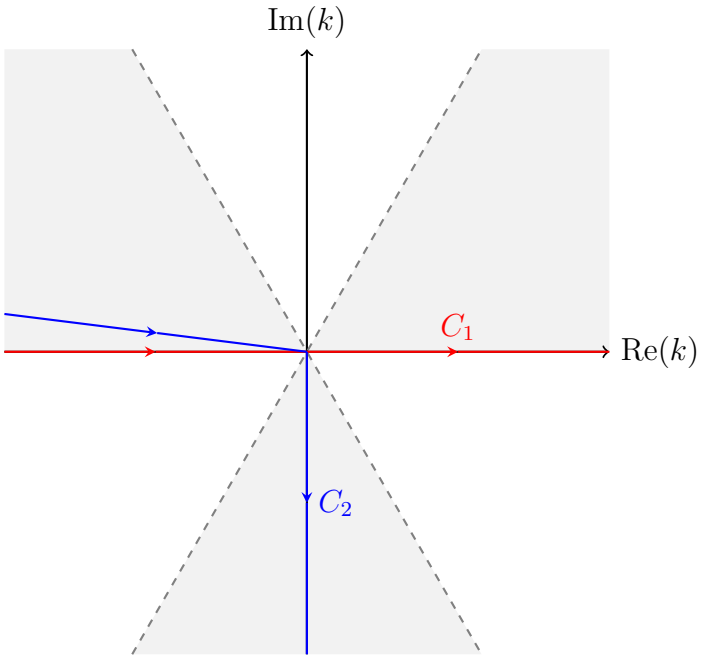

Figure 1.3: Shaded regions of (1.48) together with contours C_1 and C_2 used in derivation of the Airy functions.

If k_+ and k_- approach infinity in regions given by (1.48) (shaded regions in Figure 1.3), the boundary terms will vanish. If we take contour C_1 from Figure 1.3 running along a real line, the result is the Airy function

$$\mathrm{Ai}(u) = \int_{-\infty}^{\infty} \frac{\mathrm{d}k}{2\pi} e^{\frac{ik^3}{3}} e^{iku} = \frac{1}{\pi} \int_0^{\infty} \mathrm{d}k \, \cos\left(\frac{1}{3}k^3 + ku\right). \tag{1.49}$$

As we will see, it oscillates for negative u and decays rapidly to zero for positive u. We need another contour that cannot be deformed into C_1 to get another linearly independent solution to our second-order linear differential equation. We will use contour C_2 from Figure 1.3. The second solution $\mathrm{Bi}(u)$ is defined so it is oscillatory in the same way as $\mathrm{Ai}(u)$ for negative u, but unlike $\mathrm{Ai}(u)$ it grows

without bound for positive u. This is obtained by using the sum of contours

$$\begin{aligned}
&\mathrm{Bi}(u) = -i\int_{C_1}\frac{\mathrm{d}k}{2\pi}\,e^{\frac{ik^3}{3}}e^{iku} + 2i\int_{C_2}\frac{\mathrm{d}k}{2\pi}\,e^{\frac{ik^3}{3}}e^{iku} = \\
&= -i\int_{-\infty}^{\infty}\frac{\mathrm{d}k}{2\pi}\,e^{\frac{ik^3}{3}}e^{iku} + 2i\left(\int_{-\infty}^{0}\frac{\mathrm{d}k}{2\pi}\,e^{\frac{ik^3}{3}}e^{iku} - i\int_{0}^{\infty}\frac{\mathrm{d}k}{2\pi}\,e^{\frac{-k^3}{3}}e^{ku}\right) = \\
&= i\int_{-\infty}^{0}\frac{\mathrm{d}k}{2\pi}\,e^{\frac{ik^3}{3}}e^{iku} - i\int_{0}^{\infty}\frac{\mathrm{d}k}{2\pi}\,e^{\frac{ik^3}{3}}e^{iku} + \int_{0}^{\infty}\frac{\mathrm{d}k}{\pi}\,e^{\frac{-k^3}{3}}e^{ku} = \\
&= i\int_{0}^{\infty}\frac{\mathrm{d}k}{2\pi}\,(e^{\frac{-ik^3}{3}}e^{-iku} - e^{\frac{ik^3}{3}}e^{iku}) + \int_{0}^{\infty}\frac{\mathrm{d}k}{\pi}\,e^{\frac{-k^3}{3}}e^{ku} = \\
&= \frac{1}{\pi}\int_{0}^{\infty}\mathrm{d}k\,\left[e^{\frac{-k^3}{3}}e^{ku} + \sin\left(\frac{k^3}{3}+ku\right)\right].
\end{aligned} \tag{1.50}$$

Now we will investigate asymptotic behavior of $\mathrm{Ai}(u)$ and $\mathrm{Bi}(u)$. We have the Stokes effect for the Airy functions, meaning their asymptotic behavior can differ in different regions of the complex plane. We will start with the asymptotic expansion $u \gg 1$ of $\mathrm{Ai}(u)$ in integral form

$$\mathrm{Ai}(u) = \int_{C_1}\frac{\mathrm{d}k}{2\pi}\,e^{i\left(\frac{k^3}{3}+ku\right)}. \tag{1.51}$$

The bulk contribution to the integral comes from points k_s where the phase is stationary

$$\phi(k) = \frac{k^3}{3} + ku \quad\Rightarrow\quad \phi'(k) = k^2 + u \quad\Rightarrow\quad k_\mathrm{s} = \pm i\sqrt{u}. \tag{1.52}$$

Because no poles are present, we can shift the contour C_1 to go through the point $i\sqrt{u}$ and parametrize it with a new real variable

$$k = i\sqrt{u} + \widetilde{k},\ \widetilde{k} \in \mathbb{R}. \tag{1.53}$$

In terms of the new variable $\widetilde{k}$ we have

$$\begin{aligned}
&\phi(k) = \phi(i\sqrt{u}+\widetilde{k}) = \frac{2}{3}iu^{\frac{3}{2}} + i\sqrt{u}\widetilde{k}^2 + \frac{1}{3}\widetilde{k}^3 \\
&\mathrm{Ai}(u) = \exp\left(-\frac{2}{3}u^{\frac{3}{2}}\right)\int_{-\infty}^{\infty}\frac{\mathrm{d}\widetilde{k}}{2\pi}\,\exp(-\sqrt{u}\widetilde{k}^2 + i\widetilde{k}^3) \simeq \\
&\simeq \frac{1}{2\sqrt{\pi}}\frac{1}{u^{\frac{1}{4}}}\exp\left(-\frac{2}{3}u^{\frac{3}{2}}\right),
\end{aligned} \tag{1.54}$$

where in the last step, we ignored the $i\widetilde{k}^3$ term because it is suppressed by $-\sqrt{u}\widetilde{k}^2$ term for large u. Therefore we get the first asymptotic

$$\mathrm{Ai}(u) \simeq \frac{1}{2\sqrt{\pi}}\frac{1}{u^{\frac{1}{4}}}\exp\left(-\frac{2}{3}u^{\frac{3}{2}}\right),\ u \gg 1. \tag{1.55}$$

In the asymptotic expansion $u \ll -1$, stationary points are real, and no shift is needed; using the same technique, we get

$$\mathrm{Ai}(u) \simeq \frac{1}{\sqrt{\pi}} \frac{1}{|u|^{\frac{1}{4}}} \cos\left(\frac{2}{3}|u|^{\frac{3}{2}} - \frac{\pi}{4}\right), \; u \ll -1. \tag{1.56}$$

In the same way we get expansions for $\mathrm{Bi}(u)$

$$\mathrm{Bi}(u) \simeq \frac{1}{\sqrt{\pi}} \frac{1}{u^{\frac{1}{4}}} \exp\left(\frac{2}{3}u^{\frac{3}{2}}\right), \; u \gg 1, \tag{1.57}$$

$$\mathrm{Bi}(u) \simeq -\frac{1}{\sqrt{\pi}} \frac{1}{|u|^{\frac{1}{4}}} \sin\left(\frac{2}{3}|u|^{\frac{3}{2}} - \frac{\pi}{4}\right), \; u \ll -1. \tag{1.58}$$

Equations (1.55), (1.56) and (1.57), (1.58) are connected since they are expansions of a single object $\mathrm{Ai}(u)$ and $\mathrm{Bi}(u)$.

1.1.4 Connection formulae

Consider a general potential $V(x)$ as shown in Figure 1.4.

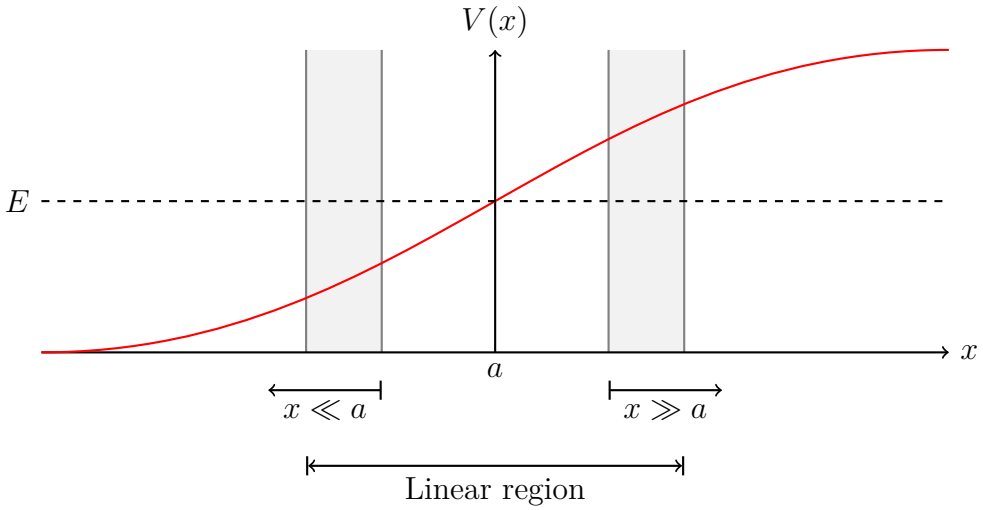

Figure 1.4: Shaded regions where the potential $V(x)$ is approximately linear and far enough from a that the WKB solutions are valid.

Near $x = a$ is the potential sufficiently linear sloping upwards and $V(x) - E$ vanishes at $x = a$, therefore

$$V(x) - E \simeq g(x - a), \; g > 0. \tag{1.59}$$

As we have seen in (1.22), WKB basic solution far to the right $x \gg a$ is

$$\psi_{\mathrm{R}}(x) = \frac{C}{\sqrt{\kappa(x)}} \exp\left(-\int_a^x \kappa(x')\,\mathrm{d}x'\right) + \frac{D}{\sqrt{\kappa(x)}} \exp\left(\int_a^x \kappa(x')\,\mathrm{d}x'\right). \tag{1.60}$$

The solution above was evaluated in (1.36) under the assumption that potential was strictly linear. If we are in the shaded regions of Figure 1.4, then we are far

enough from the turning point, but the potential is still accurately linear, and we can use (1.36) to get

$$\psi_{\mathrm{R}}(u) = \frac{C}{u^{\frac{1}{4}}} \exp\left(-\frac{2}{3}u^{\frac{3}{2}}\right) + \frac{D}{u^{\frac{1}{4}}} \exp\left(\frac{2}{3}u^{\frac{3}{2}}\right),\ u \gg 1, \tag{1.61}$$

where we used the unit free variable $u = (x-a)/L$. Similarly, we will use the WKB solution far to the left $x \ll a$ obtained in (1.20), but we will write it in terms of cosine and sine functions with phase shift of $\pi/4$ which will prove convenient

$$\psi_{\mathrm{L}}(x) = \frac{A}{\sqrt{k(x)}} \cos\left(\int_x^a k(x')\,\mathrm{d}x' - \frac{\pi}{4}\right) + \frac{B}{\sqrt{k(x)}} \sin\left(\int_x^a k(x')\,\mathrm{d}x' - \frac{\pi}{4}\right). \tag{1.62}$$

Again, using the fact that we are in a shaded region, we can use the evaluation done in (1.37) with minor modifications

$$\psi_{\mathrm{L}}(u) = \frac{A}{|u|^{\frac{1}{4}}} \cos\left(\frac{2}{3}|u|^{\frac{3}{2}} - \frac{\pi}{4}\right) + \frac{B}{|u|^{\frac{1}{4}}} \sin\left(\frac{2}{3}|u|^{\frac{3}{2}} - \frac{\pi}{4}\right),\ u \ll -1. \tag{1.63}$$

From asymptotic expansions of $\mathrm{Ai}(u)$ in (1.55) and (1.56) we know that

$$\frac{1}{2\sqrt{\pi}} \frac{1}{u^{\frac{1}{4}}} \exp\left(-\frac{2}{3}u^{\frac{3}{2}}\right) \quad \Leftrightarrow \quad \frac{1}{\sqrt{\pi}} \frac{1}{|u|^{\frac{1}{4}}} \cos\left(\frac{2}{3}|u|^{\frac{3}{2}} - \frac{\pi}{4}\right). \tag{1.64}$$

By the arrows, we mean they are asymptotic expansions of a single quantity. This implies that $C = A/2$. From asymptotic expansions of $\mathrm{Bi}(u)$ in (1.57) and (1.58) we know that

$$\frac{1}{\sqrt{\pi}} \frac{1}{u^{\frac{1}{4}}} \exp\left(\frac{2}{3}u^{\frac{3}{2}}\right) \quad \Leftrightarrow \quad -\frac{1}{\sqrt{\pi}} \frac{1}{|u|^{\frac{1}{4}}} \sin\left(\frac{2}{3}|u|^{\frac{3}{2}} - \frac{\pi}{4}\right). \tag{1.65}$$

Which implies that $D = -B$. Putting it all together and letting $A \to 2A$, we get

$$\psi_{\mathrm{R}}(x) = \frac{A}{\sqrt{\kappa(x)}} \exp\left(-\int_a^x \kappa(x')\,\mathrm{d}x'\right) - \frac{B}{\sqrt{\kappa(x)}} \exp\left(\int_a^x \kappa(x')\,\mathrm{d}x'\right), \tag{1.66}$$

$$\psi_{\mathrm{L}}(x) = \frac{2A}{\sqrt{k(x)}} \cos\left(\int_x^a k(x')\,\mathrm{d}x' - \frac{\pi}{4}\right) + \frac{B}{\sqrt{k(x)}} \sin\left(\int_x^a k(x')\,\mathrm{d}x' - \frac{\pi}{4}\right). \tag{1.67}$$

There is only one subtlety left, the direction of arrows in (1.64) and (1.65).

- Let $B = 0$ and $A = 1$, then we have

$$\frac{2}{\sqrt{k(x)}} \cos\left(\int_x^a k(x')\,\mathrm{d}x' - \frac{\pi}{4}\right) \quad \overset{?}{\Leftrightarrow} \quad \frac{1}{\sqrt{\kappa(x)}} \exp\left(-\int_a^x \kappa(x')\,\mathrm{d}x'\right). \tag{1.68}$$

  If we have an object to the right, then the arrow pointing to the left tells us correctly that we match the object to the left. However, if we have an

object to the left, there is always uncertainty that there is also sine with a small coefficient B. That implies a growing exponential that overwhelms the decaying exponential above. Therefore, the correct connection formula is

$$\frac{2}{\sqrt{k(x)}}\cos\left(\int_x^a k(x')\,\mathrm{d}x' - \frac{\pi}{4}\right) \quad \Leftarrow \quad \frac{1}{\sqrt{\kappa(x)}}\exp\left(-\int_a^x \kappa(x')\,\mathrm{d}x'\right). \tag{1.69}$$

- Let $A = 0$ and $B = -1$, then we have

$$-\frac{1}{\sqrt{k(x)}}\sin\left(\int_x^a k(x')\,\mathrm{d}x' - \frac{\pi}{4}\right) \quad \overset{?}{\Leftrightarrow} \quad \frac{1}{\sqrt{\kappa(x)}}\exp\left(\int_a^x \kappa(x')\,\mathrm{d}x'\right). \tag{1.70}$$

  If we have an object to the left, then the arrow pointing to the right tells us correctly that we match the object to the right because cosine with a small coefficient A leads to decaying exponential, which is invisible in comparison to growing exponential. However, if we have an object to the right decaying exponentially with a small coefficient A, it leads to cosine, which is comparable to sine. Therefore, the correct connection formula is

$$-\frac{1}{\sqrt{k(x)}}\sin\left(\int_x^a k(x')\,\mathrm{d}x' - \frac{\pi}{4}\right) \quad \Rightarrow \quad \frac{1}{\sqrt{\kappa(x)}}\exp\left(\int_a^x \kappa(x')\,\mathrm{d}x'\right). \tag{1.71}$$

The whole analysis above was done for a potential sloping upwards. The same arguments apply to a potential sloping downwards with a turning point at $x = b$. Connection formulae, in that case, are

$$\frac{1}{\sqrt{\kappa(x)}}\exp\left(-\int_x^b \kappa(x')\,\mathrm{d}x'\right) \quad \Rightarrow \quad \frac{2}{\sqrt{k(x)}}\cos\left(\int_b^x k(x')\,\mathrm{d}x' - \frac{\pi}{4}\right) \tag{1.72}$$

$$-\frac{1}{\sqrt{\kappa(x)}}\exp\left(\int_x^b \kappa(x')\,\mathrm{d}x'\right) \quad \Leftarrow \quad \frac{1}{\sqrt{k(x)}}\sin\left(\int_b^x k(x')\,\mathrm{d}x' - \frac{\pi}{4}\right). \tag{1.73}$$

All results can be summarized into one true statement for all cases:

> We can connect away from a decaying exponential and into a growing one.

Be careful; this is relative to the turning point. The decaying exponential decays as we move away from the turning point into the forbidden region, and the growing exponential grows as we move away from the turning point into the forbidden region.

1.1.5 Double-well potential

We will use the WKB approximation to calculate the energy splitting of the ground state and the first excited state in the double-well potential. We will work with potential

$$V(x) = \frac{m\omega^2}{8a^2}(x^2 - a^2)^2, \tag{1.74}$$

depicted in Figure 1.5.

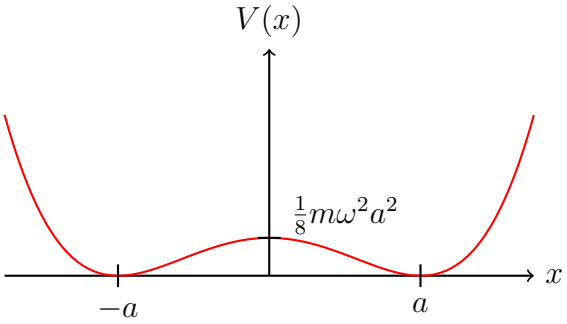

Figure 1.5: The double-well potential from (1.74).

If we expand our potential around $x = a$ in the Taylor series, we get

$$V(x) = \frac{m\omega^2}{2}(x-a)^2 + \frac{m\omega^2}{2a}(x-a)^3 + \frac{m\omega^2}{8a^2}(x-a)^4. \tag{1.75}$$

We can see that around $x = a$ wells are in the first approximation harmonic oscillators, but there is also cubic and quartic anharmonicity. More precisely, if $|x-a| \ll a$, then anharmonic corrections are small. For example, for the cubic term, we have

$$\frac{m\omega^2}{2a}|x-a|^3 = \frac{m\omega^2}{2a}(x-a)^2|x-a| \ll \frac{m\omega^2}{2}(x-a)^2. \tag{1.76}$$

Introducing length parameter $L_0 = \sqrt{\frac{\hbar}{m\omega}}$ which is the half-width of the harmonic oscillator wavefunction for its ground state energy (see Figure 1.7), we rewrite our potential in the unit free variable u and parameter λ

$$u = \frac{x}{L_0},\ \lambda = \frac{a}{L_0} \quad \Rightarrow \quad V(u) = \frac{\hbar\omega}{8}\frac{1}{\lambda^2}(u^2-\lambda^2)^2. \tag{1.77}$$

As $\lambda \to \infty$ the height of the barrier between the wells $V(0) = \frac{\hbar\omega}{8}\lambda^2$ is increasing. We will work with $V(0) \gg \hbar\omega$. In large λ approximation $L_0 \ll a$ and small anharmonicity is also satisfied when $|x-a| \gtrsim L_0$, few L_0 from $x = a$.

The ground state and the first excited state of the double-well are even and odd functions. This should not surprise us because when the barrier is large, the potential is approximately two harmonic oscillators with the same parity of the ground state and the first excited state as for the double-well. We will denote wavefunctions of the first two states as $\psi_+(x)$ and $\psi_-(x)$, where subscript refers to their parity. In the large λ limit, we will approximate $\psi_+(x)$ and $\psi_-(x)$ as an even and odd combination of two ground state wavefunctions of harmonic oscillators centered at $x = \pm a$ as depicted in Figure 1.6.

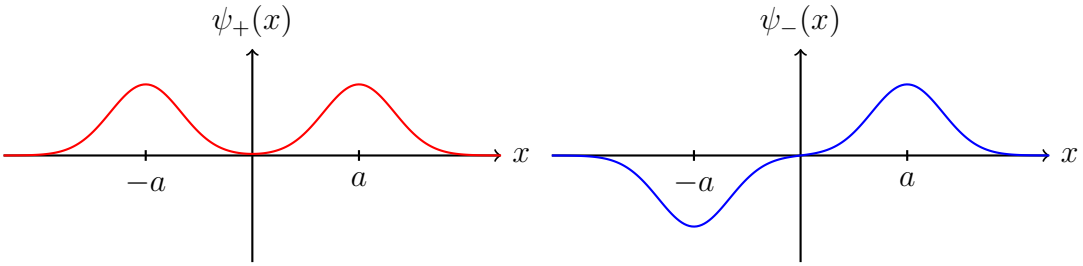

Figure 1.6: Even and odd combination of two ground state functions of the harmonic oscillator centered at $\pm a$.

This is a good approximation around $x = \pm a$ but not around $x = 0$. For exact solutions $\psi_\pm(x)$ we have

$$\hat{H}\psi_\pm(x) = E_\pm \psi_\pm(x), \tag{1.78}$$

$$E_\pm = \overline{E} \mp \frac{1}{2}\Delta E,\ \Delta E = E_- - E_+ > 0, \tag{1.79}$$

where $\psi_\pm(x)$ are orthonormal, and we assume without a loss of generality that both wavefunctions are positive for large x. It follows that $\psi_+(x) \simeq \psi_-(x)$, $x > 0$. Using this approximation, we get

$$\begin{aligned}
&-\frac{\hbar^2}{2m}\psi_+''(x) = E_+\psi_+(x),\\
&-\frac{\hbar^2}{2m}\psi_-''(x) = E_-\psi_-(x),\\
&-\frac{\hbar^2}{2m}(\psi_-''(x)\psi_+(x) - \psi_+''(x)\psi_-(x)) = \Delta E\psi_+(x)\psi_-(x),\\
&-\frac{\hbar^2}{2m}(\psi_-'(x)\psi_+(x) - \psi_+'(x)\psi_-(x))' = \Delta E\psi_+(x)\psi_-(x).
\end{aligned} \tag{1.80}$$

Integrating both sides from 0 to ∞ and using that $\psi_-(0) = 0$, $\psi_+'(0) = 0$, $\psi_\pm(\infty) = 0$, we get

$$\begin{aligned}
&\frac{\hbar^2}{2m}\psi_+(0)\psi_-'(0) = \Delta E\int_0^\infty \mathrm{d}x\,\psi_+(x)\psi_-(x),\\
&\psi_+(x) \simeq \psi_-(x),\ x > 0,\\
&\int_0^\infty \mathrm{d}x\,\psi_+(x)\psi_-(x) \simeq \int_0^\infty \mathrm{d}x\,\psi_+(x)\psi_+(x) = \frac{1}{2},\\
&\Delta E \simeq \frac{\hbar^2}{m}\psi_+(0)\psi_-'(0).
\end{aligned} \tag{1.81}$$

We will focus on single-well ground states with energy $E = \hbar\omega/2$. One of the turning points in the harmonic approximation is located at $x_1 = a - L_0$. The forbidden region extends from $-x_1$ to x_1. In the forbidden region, it holds $|x - a| \gtrsim L_0$. Therefore, we expect negligible anharmonicity. Using expression (1.22) and parity of $\psi_\pm(x)$, we can write the WKB ansatzes for wavefunctions in the

forbidden region

$$\psi_+(x) \simeq \frac{C_+}{\sqrt{\kappa(x)}} \cosh\left(\int_0^x \kappa(x')\,\mathrm{d}x'\right), \tag{1.82}$$

$$\psi_-(x) \simeq \frac{C_-}{\sqrt{\kappa(x)}} \sinh\left(\int_0^x \kappa(x')\,\mathrm{d}x'\right), \tag{1.83}$$

where it is good to remind that $\kappa^2(x) = 2m(V(x) - E)/\hbar^2$ and in this case $E = \hbar\omega/2$. We can now plug these ansatzes into equation (1.81) to get

$$\psi'_-(0) = C_-\sqrt{\kappa(0)},\ \psi_+(0) = C_+\frac{1}{\sqrt{\kappa(0)}},$$

$$\Delta E \simeq \frac{\hbar^2}{m} C_+ C_-. \tag{1.84}$$

Near $x = a$, we can write using the wavefunction of the ground state of harmonic potential $\phi_0(x)$

$$\psi_\pm(x) = \frac{1}{\sqrt{2}}(\phi_0(x-a) \pm \phi_0(x+a)), \tag{1.85}$$

$$\phi_0(x) = \frac{1}{\pi^{\frac{1}{4}}\sqrt{L_0}} \exp\left(-\frac{x^2}{2L_0^2}\right). \tag{1.86}$$

Let us focus on $x > 0$. The approximation above holds as long as $|x-a| \ll a$. On the other hand, the WKB approximation expressions in the forbidden region are valid for $|x-a| \gg L_0$ while x is to the left of a. Since in large λ approximation is $L_0 \ll a$, the condition $L_0 \ll |x-a| \ll a$ can be satisfied simultaneously. Therefore, we can match these two approximations. The region of validity is depicted in Figure 1.7 as the shaded region.

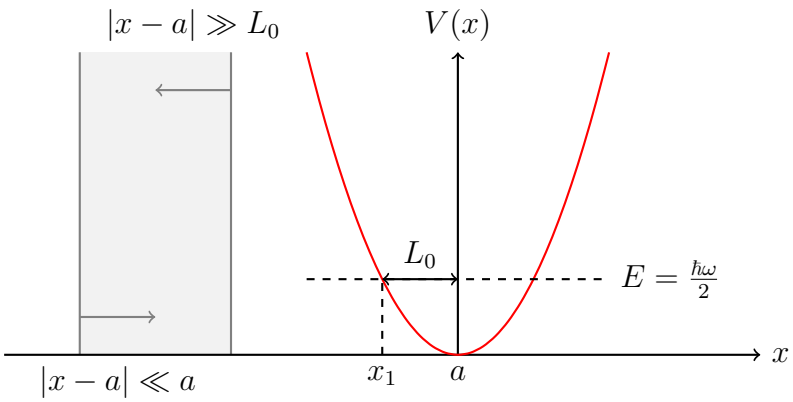

Figure 1.7: The shaded region where the potential is approximately the harmonic oscillator and not far enough from 0 that the WKB solutions are valid.

From hyperbolic functions, we must take only leading exponentials. Working with $x > 0$, only the ground state centered at $x = a$ is relevant; the other one centered at $x = -a$ is exponentially suppressed. Therefore, we get

$$\frac{C_\pm}{2\sqrt{\kappa(x)}} \exp\left(\int_0^x \kappa(x')\,\mathrm{d}x'\right) \simeq \frac{1}{\sqrt{2}}\phi_0(x-a) = \frac{\exp\left[-\frac{(x-a)^2}{2L_0^2}\right]}{\pi^{\frac{1}{4}}\sqrt{2L_0}}. \tag{1.87}$$

Working with the left-hand side

$$\int_0^x \kappa(x')\,\mathrm{d}x' = \int_0^{x_1} \kappa(x')\,\mathrm{d}x' - \int_x^{x_1} \kappa(x')\,\mathrm{d}x',$$
$$\exp\left(\int_0^x \kappa(x')\,\mathrm{d}x'\right) = \exp\left(\int_0^{x_1} \kappa(x')\,\mathrm{d}x'\right)\exp\left(-\int_x^{x_1} \kappa(x')\,\mathrm{d}x'\right). \tag{1.88}$$

For $x' \in [x, x_1]$ we have $V(x') \simeq m\omega^2(x'-a)^2/2$ which leads to more simplification

$$\int_x^{x_1} \kappa(x')\,\mathrm{d}x' = \int_x^{x_1} \sqrt{\frac{2m}{\hbar^2}\left[\frac{1}{2}m\omega^2(x'-a)^2 - \frac{1}{2}\hbar\omega\right]}\,\mathrm{d}x' =$$
$$= \int_u^{u_1} \sqrt{(\lambda-u')^2-1}\,\mathrm{d}u' = \int_1^{\lambda-u} \sqrt{t^2-1}\,\mathrm{d}t, \tag{1.89}$$

where we firstly substituted $x' = L_0u'$, giving $u_1 = \lambda - 1$, and then substituted $t = \lambda - u'$. Using the fact $a - x \gg L_0 \Leftrightarrow \lambda - u \gg 1$

$$\int_1^{\lambda-u} \sqrt{t^2-1}\,\mathrm{d}t = \frac{1}{2}(\lambda-u)\sqrt{(\lambda-u)^2-1} - \frac{1}{2}\ln\left[\lambda-u+\sqrt{(\lambda-u)^2-1}\right] \simeq$$
$$\simeq \frac{1}{2}(\lambda-u)^2 - \frac{1}{2}\ln(\lambda-u) - \frac{1}{4} - \ln\sqrt{2} + \mathcal{O}((\lambda-u)^{-2}). \tag{1.90}$$

Let us use all results and plug them into equation (1.87) to obtain

$$\exp\left(-\int_x^{x_1} \kappa(x')\,\mathrm{d}x'\right) \simeq \exp\left[-\frac{1}{2}(\lambda-u)^2 + \frac{1}{2}\ln(\lambda-u) + \frac{1}{4} + \ln\sqrt{2}\right],$$
$$\frac{C_\pm e^{\frac{1}{4}}\sqrt{2}\sqrt{\lambda-u}}{2\sqrt{\kappa(x)}}\exp\left(\int_0^{x_1} \kappa(x')\,\mathrm{d}x'\right)\exp\left[-\frac{1}{2}(\lambda-u)^2\right] \simeq \frac{\exp\left[-\frac{1}{2}(\lambda-u)^2\right]}{\pi^{\frac{1}{4}}\sqrt{2L_0}}. \tag{1.91}$$

We will rewrite $\kappa(x)$ using unit free variables and we will take advantage of $(\lambda - u) \gg 1$ to get

$$\kappa(x) = \sqrt{\frac{2m}{\hbar^2}\left(V(x) - \frac{\hbar\omega}{2}\right)} = \sqrt{\frac{2m}{\hbar^2}\left(\frac{m\omega^2}{2}(x-a)^2 - \frac{\hbar\omega}{2}\right)} =$$
$$= \frac{1}{L_0}\sqrt{(u-\lambda)^2-1} \simeq \frac{1}{L_0}(\lambda-u). \tag{1.92}$$

Using this result we get

$$\frac{C_\pm e^{\frac{1}{4}}\sqrt{L_0}}{\sqrt{2}}\exp\left(\int_0^{x_1} \kappa(x')\,\mathrm{d}x'\right) \simeq \frac{1}{\pi^{\frac{1}{4}}\sqrt{2L_0}},$$
$$C_\pm \simeq \frac{1}{(\pi e)^{\frac{1}{4}}L_0}\exp\left(-\int_0^{x_1} \kappa(x')\,\mathrm{d}x'\right). \tag{1.93}$$

Using this result in equation (1.84), we get an equation for the energy splitting of the ground state in general double-well potential

$$\Delta E \simeq \frac{\hbar\omega}{\sqrt{\pi e}}\exp\left(-2\int_0^{x_1} \kappa(x')\,\mathrm{d}x'\right). \tag{1.94}$$

The expression above generally holds for potentials that can be well approximated by single-wells at $x = \pm a$ separated by a high barrier.

Our last task is to use the expression for the energy splitting above for double-well potential (1.74). The whole task simplifies into evaluating the integral

$$I = \int_0^{x_1} \kappa(x')\,\mathrm{d}x' = \frac{1}{\hbar}\int_0^{x_1} \sqrt{2m(V(x') - E)}\,\mathrm{d}x', \tag{1.95}$$

where $E = \frac{\hbar\omega}{2}$ and $x_1 = a - L_0$. Using $b > 0$ and $L_0 \ll b \ll a$, we will split this integral to obtain

$$I = \frac{1}{\hbar}\int_0^{a-b} \sqrt{2m(V(x') - E)}\,\mathrm{d}x' + \frac{1}{\hbar}\int_{a-b}^{x_1} \sqrt{2m(V(x') - E)}\,\mathrm{d}x'. \tag{1.96}$$

It holds for $x' \in [0, a-b]$ that $E \ll V(x)$, thus first integral can be expanded keeping the first correction

$$\begin{aligned} I = \frac{1}{\hbar}\int_0^{a-b} \sqrt{2mV(x')}\,\mathrm{d}x' - \frac{1}{\hbar}\int_0^{a-b} \frac{\sqrt{m}E}{\sqrt{2V(x')}}\,\mathrm{d}x' + \\ + \frac{1}{\hbar}\int_{a-b}^{x_1} \sqrt{2m(V(x') - E)}\,\mathrm{d}x' = I_1 + I_2 + I_3. \end{aligned} \tag{1.97}$$

We will again split integral I_1 into two parts. For $x' \in [0, a]$ we will use exact form of $V(x')$ but for $x' \in [a-b, a]$ harmonic approximation holds quite well

$$\begin{aligned} I_1 = \frac{1}{\hbar}\int_0^{a} \sqrt{2m\frac{m\omega^2}{8a^2}(x'^2 - a^2)^2}\,\mathrm{d}x' - \frac{1}{\hbar}\int_{a-b}^{a} \sqrt{2m\frac{m\omega^2}{2}(x' - a)^2}\,\mathrm{d}x' = \\ = \frac{m\omega}{2\hbar a}\int_0^a (a^2 - x'^2)\,\mathrm{d}x' - \frac{m\omega}{\hbar}\int_{a-b}^a (a - x')\,\mathrm{d}x' = \frac{a^2}{3L_0^2} - \frac{b^2}{2L_0^2}. \end{aligned} \tag{1.98}$$

In calculating integral I_2 we will use exact form of $V(x')$

$$\begin{aligned} I_2 = -\frac{1}{\hbar}\int_0^{a-b} \frac{\sqrt{m}\frac{m\omega}{2}}{\sqrt{2\frac{m\omega^2}{8a^2}(x'^2 - a^2)^2}}\,\mathrm{d}x' = -a\int_0^{a-b} \frac{1}{a^2 - x'^2}\,\mathrm{d}x' = \\ = \frac{1}{2}\ln\left(\frac{b}{2a-b}\right). \end{aligned} \tag{1.99}$$

For integral I_3, we can use harmonic approximation

$$\begin{aligned} I_3 = \frac{1}{\hbar}\int_{a-b}^{x_1} \sqrt{2m\left[\frac{m\omega^2}{2}(x' - a)^2 - \frac{\hbar\omega}{2}\right]}\,\mathrm{d}x' = \\ = \sqrt{\frac{m\omega}{\hbar}}\int_{a-b}^{x_1} \sqrt{\frac{m\omega}{\hbar}(x' - a)^2 - 1}\,\mathrm{d}x' = \\ = \frac{b}{2L_0}\sqrt{\frac{b^2}{L_0^2} - 1} - \frac{1}{2}\ln\left(\frac{b}{L_0} + \sqrt{\frac{b^2}{L_0^2} - 1}\right). \end{aligned} \tag{1.100}$$

By letting $b/a \to 0$ and $L_0/b \to 0$ we obtain

$$I = I_1 + I_2 + I_3 = \frac{a^2}{3L_0^2} - \frac{b^2}{2L_0^2} + \frac{1}{2}\ln\left(\frac{b}{2a-b}\right) + \frac{b}{2L_0}\sqrt{\frac{b^2}{L_0^2}-1} -$$
$$- \frac{1}{2}\ln\left(\frac{b}{L_0} + \sqrt{\frac{b^2}{L_0^2}-1}\right) \simeq \frac{a^2}{3L_0^2} - \frac{b^2}{2L_0^2} +$$
$$+ \frac{1}{2}\ln\left(\frac{b}{2a}\right) + \frac{b^2}{2L_0^2} - \frac{1}{2}\ln\left(\frac{b}{L_0}\right) - \frac{1}{4} - \ln\sqrt{2} =$$
$$= \frac{a^2}{3L_0^2} - \frac{1}{2}\ln\left(\frac{2a}{L_0}\right) - \frac{1}{4} - \ln\sqrt{2}. \tag{1.101}$$

Plugging this result into (1.94), we get

$$\Delta E \simeq \frac{\hbar\omega}{\sqrt{\pi e}} \exp\left\{-2\left[\frac{a^2}{3L_0^2} - \frac{1}{2}\ln\left(\frac{2a}{L_0}\right) - \frac{1}{4} - \ln\sqrt{2}\right]\right\}, \tag{1.102}$$

we finally obtain an expression for the ground state energy splitting in potential (1.74). It is

$$\Delta E \simeq \frac{4\hbar\omega}{\sqrt{\pi}}\lambda \exp\left(-\frac{2}{3}\lambda^2\right). \tag{1.103}$$

From this result, we can see that in the large λ limit, when a double-well becomes two isolated wells, splitting of the ground state energy is exponentially suppressed.

1.2 Path integral around instanton

We will show the derivation of the path integral in quantum mechanics and its usage in the calculation of the partition function as was done in [4] and [3]. We will introduce an instanton concept and its effects in a double-well potential. We will approximate the path integral around instanton in a so-called one-loop approximation. In the process, we will meet the calculation of the spectrum of the Pöschl-Teller operators and their determinants. In the end, we will use the knowledge we have gained to calculate the ground-state energy splitting in the double-well potential. We will follow the steps of [5]; another works considering instantons in the double-well potential are [12] and [6].

1.2.1 Path integrals in quantum mechanics

Suppose we have a particle of mass m in a potential $V(x)$ with the quantum Hamiltonian

$$\hat{H} = \frac{\hat{p}^2}{2m} + V(\hat{x}). \tag{1.104}$$

The Hamiltonian is time-independent; therefore, we can write evolution operator simply as

$$\hat{U}(t_\mathrm{f}, t_\mathrm{i}) = \exp\left[-\frac{i}{\hbar}\hat{H}(t_\mathrm{f} - t_\mathrm{i})\right], \tag{1.105}$$

where $t_\mathrm{i} < t_\mathrm{f}$ is initial and final time, we will denote $T = (t_\mathrm{f} - t_\mathrm{i})$. We will calculate the kernel of the evolution operator, also known as the propagator

$$\mathcal{K}(x_\mathrm{f}, t_\mathrm{f}, x_\mathrm{i}, t_\mathrm{i}) = \langle x_\mathrm{f}| \hat{U}(t_\mathrm{f}, t_\mathrm{i})|x_\mathrm{i}\rangle. \tag{1.106}$$

The propagator is a probability amplitude that a particle localized at position x_i at time t_i will be localized at position x_f at a later time t_f. We will show that the propagator can be written as

$$\mathcal{K}(x_\mathrm{f}, t_\mathrm{f}, x_\mathrm{i}, t_\mathrm{i}) = \sum_{\substack{\text{paths } x(t) \\ x(t_\mathrm{i})=x_\mathrm{i} \\ x(t_\mathrm{f})=x_\mathrm{f}}} \exp\left(\frac{i}{\hbar} S[x(t)]\right), \tag{1.107}$$

whereby the sum we mean integral over space of classical trajectories in configuration space with given endpoints and $S[x(t)]$ is the classical action of the particle as a functional of its trajectory $x(t)$.

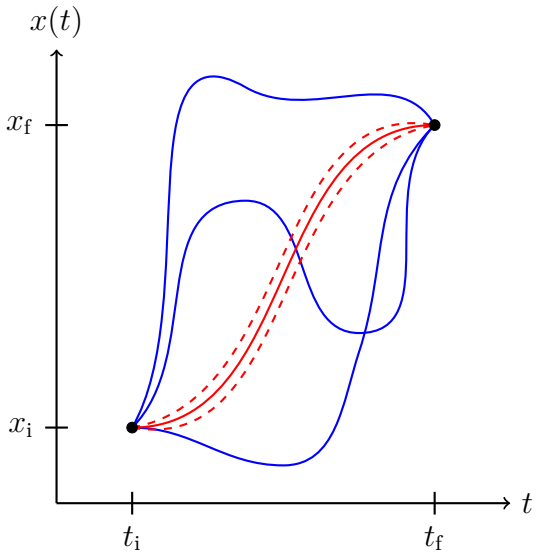

Figure 1.8: Some of the possible paths from $(t_\mathrm{i}, x_\mathrm{i})$ to $(t_\mathrm{f}, x_\mathrm{f})$. The biggest contribution to the functional integral is from trajectories in the vicinity of the classical trajectory (red), for which $\delta S = 0$. These contribute in phase while others (blue) tend to cancel each other.

We will start with a free particle with the Hamiltonian

$$\hat{H}_0 = \frac{\hat{p}^2}{2m}. \tag{1.108}$$

To calculate the free propagator $\mathcal{K}_0(x_\mathrm{f}, x_\mathrm{i}, T) = \langle x_\mathrm{f}| \exp\left(-\frac{i}{\hbar}\hat{H}_0 T\right)|x_\mathrm{i}\rangle$ we will use decomposition of the identity operator into momentum states $\hat{I} = \int \mathrm{d}p\, |p\rangle\langle p|$ and

integration of Gaussian function

$$\begin{aligned}
&\mathcal{K}_0(x_\mathrm{f}, x_\mathrm{i}, T) = \langle x_\mathrm{f}| \exp\left(-\frac{i}{\hbar}\frac{\hat{p}^2}{2m}T\right)|x_\mathrm{i}\rangle = \\
&= \langle x_\mathrm{f}| \exp\left(-\frac{i}{\hbar}\frac{\hat{p}^2}{2m}T\right)\hat{I}|x_\mathrm{i}\rangle = \\
&= \int \mathrm{d}p\, \exp\left(-\frac{i}{\hbar}\frac{p^2}{2m}T\right)\langle x_\mathrm{f}|p\rangle\langle p|x_\mathrm{i}\rangle = \\
&= \int \frac{\mathrm{d}p}{2\pi\hbar}\, \exp\left[-\frac{i}{\hbar}\frac{p^2}{2m}T + \frac{i}{\hbar}p(x_\mathrm{f}-x_\mathrm{i})\right] = \\
&= \frac{1}{2\pi\hbar}\sqrt{\pi\frac{2m\hbar}{Ti}}\exp\left\{-\left[\frac{i}{\hbar}(x_\mathrm{f}-x_\mathrm{i})\right]^2\left(\frac{-2m\hbar}{4iT}\right)\right\} = \\
&= \sqrt{\frac{m}{2\pi i\hbar T}}\exp\left[\frac{im}{2\hbar T}(x_\mathrm{f}-x_\mathrm{i})^2\right]. \qquad (1.109)
\end{aligned}$$

We will proceed to calculate the full propagator. We will need the Lie-Trotter product formula, which states that for bounded not necessarily commuting operators $\hat{A}$, $\hat{B}$ on Hilbert space, we can write

$$\exp(\hat{A}+\hat{B}) = \lim_{N\to\infty}\left[\exp\left(\frac{\hat{A}}{N}\right)\exp\left(\frac{\hat{B}}{N}\right)\right]^N, \qquad (1.110)$$

where the limit is in the sense of norm convergence of operators. A similar formula is true for unbounded operators; details are in [7]. Thus, we can write

$$\begin{aligned}
&\langle x_\mathrm{f}| \exp\left[-\frac{i}{\hbar}\left(\frac{\hat{p}^2}{2m}+V(\hat{x})\right)T\right]|x_\mathrm{i}\rangle = \\
&= \lim_{\substack{N\to\infty \\ \varepsilon\to 0 \\ N\varepsilon=T}} \langle x_\mathrm{f}|\left[\exp\left(-\frac{i}{\hbar}\frac{\hat{p}^2}{2m}\varepsilon\right)\exp\left(-\frac{i}{\hbar}V(\hat{x})\varepsilon\right)\right]^N|x_\mathrm{i}\rangle. \qquad (1.111)
\end{aligned}$$

In the expression above, we have a product of N brackets; each bracket is the product of two exponential functions. In each bracket, we will insert a decomposition of the identity operator into momentum states between exponential functions. From the right of each bracket (except for the last one), we will stick a decomposition of the identity operator into position states. The j-th bracket will look like

$$\begin{aligned}
&\int\int \mathrm{d}p_j \mathrm{d}x_{j-1}\, \langle x_j| \exp\left(-\frac{i}{\hbar}\frac{\hat{p}^2}{2m}\varepsilon\right)|p_j\rangle\langle p_j| \exp\left(-\frac{i}{\hbar}V(\hat{x})\varepsilon\right)|x_{j-1}\rangle = \\
&= \int \frac{\mathrm{d}p_j \mathrm{d}x_{j-1}}{2\pi\hbar}\exp\left[-\frac{i}{\hbar}\left(\frac{p_j^2}{2m}\varepsilon + V(x_{j-1})\varepsilon - p_j(x_j-x_{j-1})\right)\right], \qquad (1.112)
\end{aligned}$$

where, for brevity, we put just one integral sign instead of two. Putting it all together, we get the expression for the full propagator

$$\begin{aligned}
&\mathcal{K}(x_\mathrm{f}, x_\mathrm{i}, T) = \\
&= \lim_{\substack{N\to\infty \\ \varepsilon\to 0 \\ N\varepsilon=T}} \int \frac{\mathrm{d}p_N}{2\pi\hbar}\left(\prod_{j=1}^{N-1}\frac{\mathrm{d}p_j\mathrm{d}x_j}{2\pi\hbar}\right)\exp\left[\frac{i}{\hbar}\sum_{k=1}^{N} p_k\frac{(x_k-x_{k-1})}{\varepsilon}\varepsilon - H(p_k, x_{k-1})\varepsilon\right], \qquad (1.113)
\end{aligned}$$

where $x_0 = x_\mathrm{i}$, $x_N = x_\mathrm{f}$. Let us interpret the obtained result above. If we have a particle with position $x(t)$ and momentum $p(t)$ its action is

$$S[x(t), p(t)] = \int_{t_\mathrm{i}}^{t_\mathrm{f}} (p(t)\dot{x}(t) - H(p(t), x(t)))\,\mathrm{d}t. \tag{1.114}$$

If we discretize $x(t)$ and $p(t)$ as in Figure 1.9 we get for $t \in (t_{j-1}, t_j)$

$$\begin{aligned} &\dot{x}(t) = \frac{x_j - x_{j-1}}{\varepsilon} \quad \Rightarrow \quad \int_{t_{j-1}}^{t_j} p(t)\dot{x}(t)\,\mathrm{d}t = p_j \frac{x_j - x_{j-1}}{\varepsilon}\varepsilon, \\ &\int_{t_{j-1}}^{t_j} \frac{p^2(t)}{2m}\,\mathrm{d}t = \frac{p_j^2}{2m}\varepsilon, \end{aligned} \tag{1.115}$$

where $\varepsilon = t_j - t_{j-1}$. We can see that in the limit $N \to \infty$, $\varepsilon \to 0$, $N\varepsilon = T$ we get

$$\sum_{k=1}^{N} p_k \frac{(x_k - x_{k-1})}{\varepsilon}\varepsilon - H(p_k, x_{k-1})\varepsilon \to \int_{t_\mathrm{i}}^{t_\mathrm{f}} (p(t)\dot{x}(t) - H(p(t), x(t)))\,\mathrm{d}t. \tag{1.116}$$

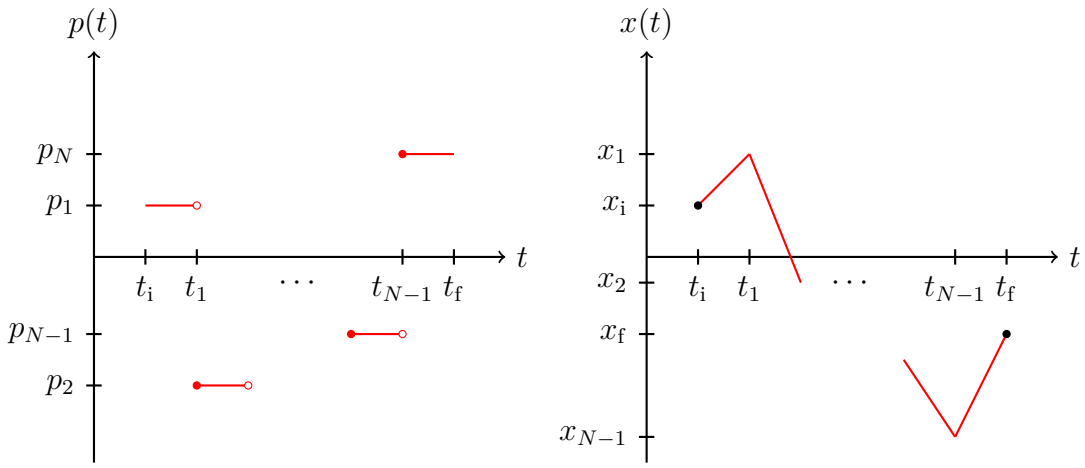

Figure 1.9: Discretization of particle's trajectory $x(t)$ and momentum $p(t)$.

Therefore, the propagator in (1.113) resembles the Riemann sum for an integral over the phase space of trajectories. This motivates us to rewrite the propagator

$$\begin{aligned} &\mathcal{K}(x_\mathrm{f}, x_\mathrm{i}, T) = \\ &= \int_{x(t_\mathrm{i})=x_\mathrm{i}}^{x(t_\mathrm{f})=x_\mathrm{f}} \mathcal{D}x(t)\mathcal{D}p(t)\, \exp\left[\frac{i}{\hbar}\left(\int_{t_\mathrm{i}}^{t_\mathrm{f}} (p(t)\dot{x}(t) - H(p(t), x(t)))\,\mathrm{d}t\right)\right], \end{aligned} \tag{1.117}$$

this is to be understood as a symbolic way of writing the Riemann sum from (1.113). It is only symbolic because $\mathcal{D}x(t)$ and $\mathcal{D}p(t)$ are not mathematically rigorous measures in the space of continuous functions. Nevertheless, the whole formalism can be reformulated such that the path integral will be a functional integral with rigorously defined measures on continuous functions (see Wiener measure in [4]).

In our case, the dependence of the Hamiltonian on momentum is just quadratic, and we can integrate the "momentum part" of (1.113), giving us "free propagator term" from (1.109). We obtain

$$\int \frac{\mathrm{d}p_N}{2\pi\hbar}\left(\prod_{j=1}^{N-1}\frac{\mathrm{d}p_j\mathrm{d}x_j}{2\pi\hbar}\right)\exp\left[\frac{i}{\hbar}\sum_{k=1}^{N}p_k\frac{(x_k-x_{k-1})}{\varepsilon}\varepsilon - H(p_k,x_{k-1})\varepsilon\right] =$$
$$= \left(\frac{m}{2\pi i\hbar\varepsilon}\right)^{\frac{N}{2}}\int\left(\prod_{j=1}^{N-1}\mathrm{d}x_j\right)\exp\left[\frac{i}{\hbar}\sum_{k=1}^{N}\frac{1}{2}m\frac{(x_k-x_{k-1})^2}{\varepsilon} - V(x_{k-1})\varepsilon\right]. \quad (1.118)$$

Again, we can use symbolic notation and rewrite the propagator

$$\begin{aligned}
&\mathcal{K}(x_\mathrm{f},x_\mathrm{i},T) = \\
&= \lim_{\substack{N\to\infty\\ \varepsilon\to 0\\ N\varepsilon=T}}\left(\frac{m}{2\pi i\hbar\varepsilon}\right)^{\frac{N}{2}}\int\left(\prod_{j=1}^{N-1}\mathrm{d}x_j\right)\exp\left[\frac{i}{\hbar}\sum_{k=1}^{N}\frac{1}{2}m\frac{(x_k-x_{k-1})^2}{\varepsilon} - V(x_{k-1})\varepsilon\right] = \\
&= \int_{x(t_\mathrm{i})=x_\mathrm{i}}^{x(t_\mathrm{f})=x_\mathrm{f}}\mathcal{D}x(t)\,\exp\left[\frac{i}{\hbar}\left(\int_{t_\mathrm{i}}^{t_\mathrm{f}}\frac{1}{2}m\dot{x}^2(t) - V(x(t))\,\mathrm{d}t\right)\right] = \\
&= \int_{x(t_\mathrm{i})=x_\mathrm{i}}^{x(t_\mathrm{f})=x_\mathrm{f}}\mathcal{D}x(t)\,\exp\left(\frac{i}{\hbar}\int_{t_\mathrm{i}}^{t_\mathrm{f}}L(x(t),\dot{x}(t))\,\mathrm{d}t\right) = \\
&= \int_{x(t_\mathrm{i})=x_\mathrm{i}}^{x(t_\mathrm{f})=x_\mathrm{f}}\mathcal{D}x(t)\,\exp\left(\frac{i}{\hbar}S[x(t)]\right), \qquad (1.119)
\end{aligned}$$

which gives us the path integral in its most famous form

$$\mathcal{K}(x_\mathrm{f},x_\mathrm{i},T) = \int_{x(t_\mathrm{i})=x_\mathrm{i}}^{x(t_\mathrm{f})=x_\mathrm{f}}\mathcal{D}x(t)\,\exp\left(\frac{i}{\hbar}S[x(t)]\right). \qquad (1.120)$$

We will show how to use the path integral in calculating the canonical partition function. To do so, we need to do something seemingly crazy. We will perform Wick rotation – the analytic continuation to imaginary time $t \to -i\tau$, where $\tau \in \mathbb{R}$. We can immediately see that it bears fruit when we write the Wick rotated evolution operator

$$\hat{U}(t_\mathrm{f},t_\mathrm{i}) = \exp\left[-\frac{i}{\hbar}\hat{H}(t_\mathrm{f}-t_\mathrm{i})\right] \to \hat{U}(\tau_\mathrm{f},\tau_\mathrm{i}) = \exp\left[-\frac{1}{\hbar}\hat{H}(\tau_\mathrm{f}-\tau_\mathrm{i})\right] \propto \hat{\rho}(\beta), \quad (1.121)$$

where we identified inverse temperature with Wick rotated time $\beta = \frac{1}{\hbar}(\tau_\mathrm{f}-\tau_\mathrm{i})$ to get an expression proportional to the canonical density operator $\hat{\rho}(\beta)$. To Wick rotate the propagator, we must substitute $\varepsilon \to -i\varepsilon$ in the discretized expression

$$\begin{aligned}
&\mathcal{K}(x_\mathrm{f},x_\mathrm{i},-i\hbar\beta) = \\
&= \lim_{\substack{N\to\infty\\ \varepsilon\to 0\\ N\varepsilon=\hbar\beta}}\left(\frac{m}{2\pi\hbar\varepsilon}\right)^{\frac{N}{2}}\int\left(\prod_{j=1}^{N-1}\mathrm{d}x_j\right)\exp\left[-\frac{1}{\hbar}\sum_{k=1}^{N}\frac{1}{2}m\frac{(x_k-x_{k-1})^2}{\varepsilon} + V(x_{k-1})\varepsilon\right] = \\
&= \int_{x(\tau_\mathrm{i})=x_\mathrm{i}}^{x(\tau_\mathrm{f})=x_\mathrm{f}}\mathcal{D}x(\tau)\,\exp\left[-\frac{1}{\hbar}\left(\int_{\tau_\mathrm{i}}^{\tau_\mathrm{f}}\frac{1}{2}m\dot{x}^2(\tau) + V(x(\tau))\,\mathrm{d}\tau\right)\right] = \\
&= \int_{x(\tau_\mathrm{i})=x_\mathrm{i}}^{x(\tau_\mathrm{f})=x_\mathrm{f}}\mathcal{D}x(\tau)\,\exp\left(-\frac{1}{\hbar}\int_{\tau_\mathrm{i}}^{\tau_\mathrm{f}}L_\mathrm{E}(x(\tau),\dot{x}(\tau))\,\mathrm{d}\tau\right) = \\
&= \int_{x(\tau_\mathrm{i})=x_\mathrm{i}}^{x(\tau_\mathrm{f})=x_\mathrm{f}}\mathcal{D}x(\tau)\,\exp\left(-\frac{1}{\hbar}S_\mathrm{E}[x(\tau)]\right), \qquad (1.122)
\end{aligned}$$

where the classical action $S[x(t)]$ changed into so-called Euclidean action $S_{\mathrm{E}}[x(\tau)]$. Calculation of the canonical partition function $Z(\beta)$ is now straightforward

$$\begin{aligned} Z(\beta) &= \mathrm{Tr}[\exp(-\hat{H}\beta)] = \int \mathrm{d}x \, \langle x| \exp(-\hat{H}\beta)|x\rangle = \int \mathrm{d}x \, \mathcal{K}(x,x,-i\hbar\beta) = \\ &= \int \mathrm{d}x \int_{x(\tau_{\mathrm{i}})=x}^{x(\tau_{\mathrm{f}})=x} \mathcal{D}x(\tau) \, \exp\left(-\frac{1}{\hbar} S_{\mathrm{E}}[x(\tau)]\right) = \\ &= \int_{x(\tau_{\mathrm{i}})=x(\tau_{\mathrm{f}})} \mathcal{D}x(\tau) \, \exp\left(-\frac{1}{\hbar} S_{\mathrm{E}}[x(\tau)]\right), \end{aligned} \tag{1.123}$$

giving us the canonical partition function in the path integral formulation

$$Z(\beta) = \int_{x(\tau_{\mathrm{i}})=x(\tau_{\mathrm{f}})} \mathcal{D}x(\tau) \, \exp\left(-\frac{1}{\hbar} S_{\mathrm{E}}[x(\tau)]\right). \tag{1.124}$$

By the last integral, we mean the integral over all periodic trajectories with the period $\hbar\beta$.

1.2.2 Instanton

The nontrivial solutions of the Euclidean equation of motion are called instantons. In other words, nontrivial solutions of

$$\delta S_{\mathrm{E}}[x(\tau)] = 0. \tag{1.125}$$

Our focus will be on instanton effects, which are non-perturbative effects that go as

$$\exp\left(-\frac{A}{g}\right), \tag{1.126}$$

where A is some constant and $g > 0$ is the coupling constant, giving us the strength of an anharmonicity. Instanton effects cause tunneling through potential barriers. Perturbed harmonic potential with unstable or false vacuum depicted in Figure 1.10 on the left does not admit bound states because of tunneling. However, it admits resonant states, which can be defined by considering scattering in the potential depicted in Figure 1.10 on the left. As a boundary condition, we demand cancellation of the incoming wavefunction (the Gamow-Siegert boundary condition). The energies of these resonant states turn out to be complex

$$E = \mathrm{Re}(E) + i\mathrm{Im}(E) = \mathrm{Re}(E) - i\frac{\Gamma}{2}, \, \Gamma > 0, \tag{1.127}$$

which is not that surprising considering standard time evolution

$$\exp\left(-\frac{i}{\hbar}Et\right) = \exp\left(-\frac{i}{\hbar}\mathrm{Re}(E)t\right) \exp\left(-\frac{\Gamma}{2\hbar}t\right), \tag{1.128}$$

where $\hbar/\Gamma$ represents the lifetime of these unstable states. In particular, the imaginary part of the ground state energy has a typical instanton effect dependence

$$\mathrm{Im}(E_0)(g) \sim \exp\left(-\frac{A}{g}\right), \tag{1.129}$$

while the real part of the ground state energy is the result obtained by the stationary perturbation theory. This is true since it is the perturbed harmonic oscillator, and for the $g \to 0$ limit, we must have

$$\mathrm{Re}(E_0) \to \hbar\omega \left(n + \frac{1}{2}\right), \; n \in \mathbb{N} \cup \{0\}. \tag{1.130}$$

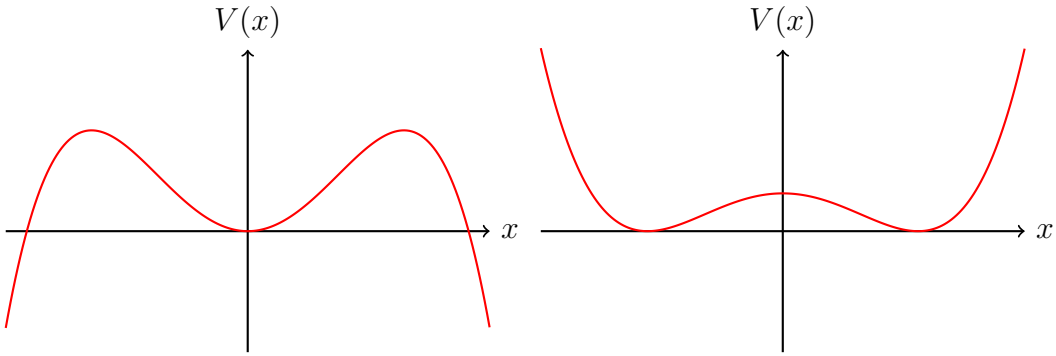

Figure 1.10: Left: the potential with unstable vacuum. Right: the double-well potential.

We will be interested in a particle in the double-well potential depicted in Figure 1.10 on the right. The perturbative method gives us twofold degenerate ground state energy; however, in reality, degeneracy is lifted due to instanton effects

$$E_1(g) - E_0(g) \sim \exp\left(-\frac{A}{g}\right). \tag{1.131}$$

From now on, we will set $\hbar = 1$, $\omega = 1$, $m = 1$, and we will work with the double-well potential of the form

$$V(x) = \frac{g}{2}\left(x^2 - \frac{1}{4g}\right)^2, \; g > 0. \tag{1.132}$$

The Euclidean action of our particle is

$$S_{\mathrm{E}}[x(\tau)] = \int_{-\beta/2}^{\beta/2} \mathrm{d}\tau \, \left(\frac{1}{2}\dot{x}^2(\tau) + V(x(\tau))\right), \tag{1.133}$$

where without loss of generality we set $\tau_{\mathrm{i}} = -\beta/2$ and $\tau_{\mathrm{f}} = \beta/2$. Calculating variation of the Euclidean action

$$\begin{aligned}
\delta S_{\mathrm{E}} &= \int_{-\beta/2}^{\beta/2} \mathrm{d}\tau \, \left(\dot{x}\delta\dot{x} + V'(x)\delta x\right) = \\
&= \left[\dot{x}\delta x\right]_{-\beta/2}^{\beta/2} + \int_{-\beta/2}^{\beta/2} \mathrm{d}\tau \, \left(-\ddot{x}\delta x + V'(x)\delta x\right) = \\
&= \int_{-\beta/2}^{\beta/2} \mathrm{d}\tau \, \left(-\ddot{x} + V'(x)\right)\delta x,
\end{aligned} \tag{1.134}$$

we get the Euclidean equation of motion

$$\begin{aligned}
\ddot{x} - V'(x) &= 0, \\
\ddot{x} - 2gx\left(x^2 - \frac{1}{4g}\right) &= 0, \\
\ddot{x} + \frac{1}{2}x - 2gx^3 &= 0.
\end{aligned} \tag{1.135}$$

The solution to this kind of nonlinear second-order differential equation is generally called the Jacobi elliptic function. We will be interested in boundary conditions $x(-\beta/2) = -x(\beta/2)$ and in the limit $\beta \to \infty$ which will be explained later. In that case, the nontrivial solution becomes simpler

$$x_{\text{in}}^{\tau_0}(\tau) = \pm \frac{1}{2\sqrt{g}} \tanh\left(\frac{\tau - \tau_0}{2}\right), \tag{1.136}$$

where we got families of solutions true for $\tau_0 \in [-\beta/2, \beta/2]$ arbitrary. The parameter τ_0 is called the modulus or the collective coordinate (it is a general feature, tied not only to the double-well potential). These families of solutions are called instanton and anti-instanton with center τ_0 for potential (1.132) and are depicted in Figure 1.11. They connect minima of our potential in $\tau = -\infty$ and $\tau = \infty$.

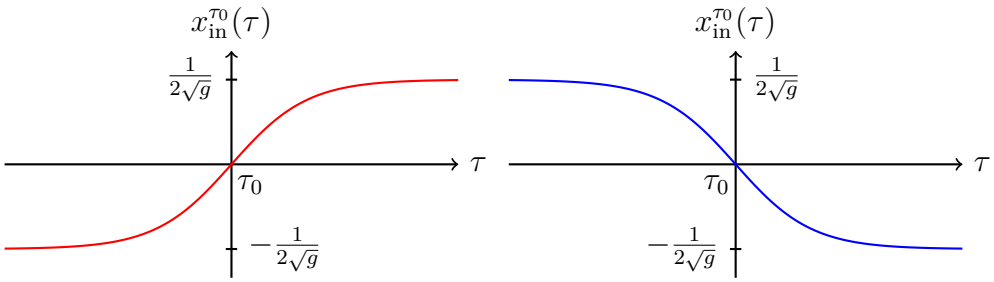

Figure 1.11: Left: instanton with the center τ_0. Right: anti-instanton with the center τ_0.

We can quickly check that, for example, the instanton solution satisfies our equation of motion

$$\begin{aligned}
&\ddot{x}_{\text{in}}^{\tau_0} + \frac{1}{2} x_{\text{in}}^{\tau_0} - 2g(x_{\text{in}}^{\tau_0})^3 = \\
&= -\frac{1}{4\sqrt{g}} \frac{\sinh\left(\frac{\tau-\tau_0}{2}\right)}{\cosh^3\left(\frac{\tau-\tau_0}{2}\right)} + \frac{1}{4\sqrt{g}} \frac{\sinh\left(\frac{\tau-\tau_0}{2}\right)}{\cosh\left(\frac{\tau-\tau_0}{2}\right)} - \frac{1}{4\sqrt{g}} \frac{\sinh^3\left(\frac{\tau-\tau_0}{2}\right)}{\cosh^3\left(\frac{\tau-\tau_0}{2}\right)} = \\
&= -\frac{1}{4\sqrt{g}} \frac{\sinh\left(\frac{\tau-\tau_0}{2}\right)\left[1 + \sinh^2\left(\frac{\tau-\tau_0}{2}\right)\right]}{\cosh^3\left(\frac{\tau-\tau_0}{2}\right)} + \frac{1}{4\sqrt{g}} \frac{\sinh\left(\frac{\tau-\tau_0}{2}\right)}{\cosh\left(\frac{\tau-\tau_0}{2}\right)} = \\
&= -\frac{1}{4\sqrt{g}} \frac{\sinh\left(\frac{\tau-\tau_0}{2}\right)}{\cosh\left(\frac{\tau-\tau_0}{2}\right)} + \frac{1}{4\sqrt{g}} \frac{\sinh\left(\frac{\tau-\tau_0}{2}\right)}{\cosh\left(\frac{\tau-\tau_0}{2}\right)} = 0.
\end{aligned} \tag{1.137}$$

Lagrangian is not explicitly dependent on time; because of that, all trajectories have to satisfy the energy conservation

$$E = \frac{\partial L_{\text{E}}}{\partial \dot{x}} \dot{x} - L_{\text{E}} = \frac{1}{2}\dot{x}^2 - V(x), \tag{1.138}$$

and action along an instanton trajectory using the above equation can be written as

$$S_{\text{E}}[x_{\text{in}}^{\tau_0}(\tau)] = S_{\text{in}} = \int_{-\beta/2}^{\beta/2} \mathrm{d}\tau (\dot{x}_{\text{in}}^{\tau_0}(\tau))^2 - E\beta = \mathcal{W}(E) - E\beta. \tag{1.139}$$

For a trajectory of the period $\beta \to \infty$ we get that energy of a particle has to be $E = 0$ (see Figure 1.12), therefore in large β limit we get

$$\mathcal{W}(0) = S_{\text{in}}. \tag{1.140}$$

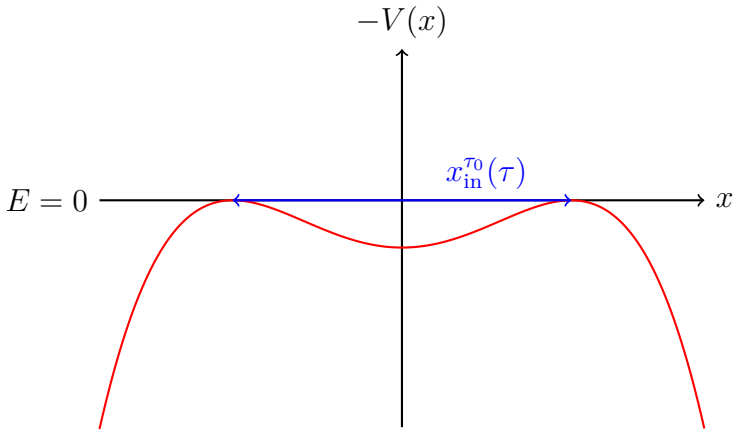

Figure 1.12: After Wick rotation, the Euclidean Hamiltonian has opposite sign before the potential as is usual, $H_{\text{E}}(x(\tau), p(\tau)) = \frac{1}{2}p^2(\tau) - V(x(\tau))$. This can be interpreted as the normal Hamiltonian of a particle moving in an inverted potential $-V(x)$. In the picture is depicted $x_{\text{in}}^{\tau_0}(\tau)$ in $\beta \to \infty$ limit.

1.2.3 One-loop approximation

This section will look at an approximation technique for calculating the path integrals. We will work with the potential from Figure 1.10 on the left

$$V(x) = \frac{1}{2}x^2 + \frac{1}{4}gx^4,\ g < 0. \tag{1.141}$$

We will be mainly interested in the double-well potential from Figure 1.10, but as we will see, unstable potentials with resonant states represent, in some sense, a more general problem.

To understand the canonical partition function expressed through the path integral for the above potential, we will focus on a toy model – a reduction from one dimension (the only dimension is time) to zero dimensions. The path integral becomes an ordinary integral

$$I(g) = \frac{1}{\sqrt{2\pi}} \int_{-\infty}^{\infty} \mathrm{d}x\, \exp\left(-\frac{1}{2}x^2 - \frac{1}{4}gx^4\right). \tag{1.142}$$

We want to calculate this integral for $g < 0$, but we can see that the integral is not convergent for $g < 0$. What to do? We will start by taking g and x to be generally complex. The idea is that we start with $g > 0$ for which we can calculate the integral and then move in complex g plane towards negative g. The integral is convergent when

$$\text{Re}(gx^4) > 0 \quad \Rightarrow \quad \text{Arg}(x) = -\frac{1}{4}\text{Arg}(g). \tag{1.143}$$

This can be achieved by rotating an integration contour as in Figure 1.13. In this way, we obtain the analytic continuation of the integral, but the resulting

function has a branch cut along negative values of g. Functions $I(-|g|+i0)$ and $I(-|g|-i0)$ are complex conjugate, thus for the discontinuity we have

$$\begin{aligned}&\pm\left(I(-|g|+i0)-I(-|g|-i0)\right)=2i\mathrm{Im}(I(g))=\\&=\frac{1}{\sqrt{2\pi}}\int_{\pm(C_+-C_-)}\mathrm{d}x\,\exp\left(-\frac{1}{2}x^2-\frac{1}{4}gx^4\right),\end{aligned}\tag{1.144}$$

where we have to choose one of the branch cuts (we will comment on that later).

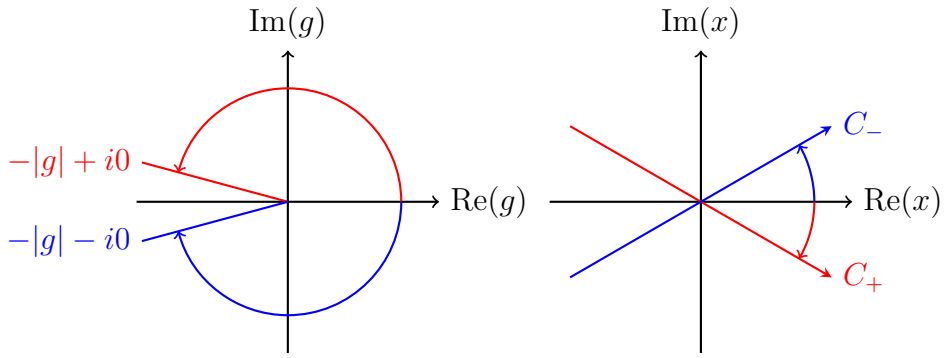

Figure 1.13: As we are approaching negative g from above and below we must rotate integration contour C_+ to $-\pi/4$ and C_- to $\pi/4$.

The discontinuity can be calculated by integrating through the nontrivial saddle points (see [5], [8] and [9]). The moral of this toy model is that by approximating the path integral for the unstable potential using nontrivial saddle points, we get the discontinuity which is equal to $2i\mathrm{Im}(Z(\beta))$. And this is exactly what we will do in the following.

We will expand the Euclidean action of a particle around the instanton solution to second-order fluctuations

$$x(\tau)=x_{\mathrm{in}}^{\tau_0}(\tau)+r(\tau),\tag{1.145}$$

$$S_{\mathrm{E}}[x(\tau)]\approx S_{\mathrm{in}}+\frac{1}{2}\int\mathrm{d}\tau_1\mathrm{d}\tau_2\,r(\tau_1)M(\tau_1,\tau_2)r(\tau_2),\tag{1.146}$$

where linear term vanishes because the instanton solves the equation of motion and $M(\tau_1,\tau_2)$ is given by

$$\begin{aligned}M(\tau_1,\tau_2)&=\left.\frac{\delta^2 S_{\mathrm{E}}}{\delta x(\tau_1)\delta x(\tau_2)}\right|_{x(\tau)=x_{\mathrm{in}}^{\tau_0}}=\\&=\frac{\delta}{\delta x(\tau_1)}\left[\frac{\partial L_{\mathrm{E}}}{\partial x(\tau_2)}-\frac{\mathrm{d}}{\mathrm{d}\tau_2}\left(\frac{\partial L_{\mathrm{E}}}{\partial\dot{x}(\tau_2)}\right)\right]\Bigg|_{x(\tau)=x_{\mathrm{in}}^{\tau_0}}=\\&=\left[\frac{\partial^2 L_{\mathrm{E}}}{\partial x(\tau_1)\partial x(\tau_2)}\delta(\tau_1-\tau_2)+\frac{\partial^2 L_{\mathrm{E}}}{\partial\dot{x}(\tau_1)\partial x(\tau_2)}\dot{\delta}(\tau_1-\tau_2)-\right.\\&\left.-\frac{\mathrm{d}}{\mathrm{d}\tau_2}\left(\frac{\partial^2 L_{\mathrm{E}}}{\partial\dot{x}(\tau_1)\partial\dot{x}(\tau_2)}\dot{\delta}(\tau_1-\tau_2)+\frac{\partial^2 L_{\mathrm{E}}}{\partial x(\tau_1)\partial\dot{x}(\tau_2)}\delta(\tau_1-\tau_2)\right)\right]\Bigg|_{x(\tau)=x_{\mathrm{in}}^{\tau_0}}=\\&=\left[-\left(\frac{\mathrm{d}}{\mathrm{d}\tau_1}\right)^2+V''(x_{\mathrm{in}}^{\tau_0}(\tau_1))\right]\delta(\tau_1-\tau_2).\end{aligned}\tag{1.147}$$

$M(\tau_1, \tau_2)$ is the integral kernel of differential operator $\mathbf{M}$ written explicitly as

$$\mathbf{M} = -\left(\frac{\mathrm{d}}{\mathrm{d}\tau}\right)^2 + V''(x_{\mathrm{in}}^{\tau_0}(\tau)). \tag{1.148}$$

In this second-order approximation, also called one-loop approximation (Feynman diagrams jargon) we have

$$\begin{aligned} &2i\mathrm{Im}(Z(\beta)) \approx \\ &\approx \exp(-S_{\mathrm{in}}) \int_{r(-\beta/2)=r(\beta/2)} \mathcal{D}r(\tau)\, \exp\left(-\frac{1}{2}\int_{-\beta/2}^{\beta/2} \mathrm{d}\tau_1 \mathrm{d}\tau_2\, r(\tau_1) M(\tau_1, \tau_2) r(\tau_2)\right), \end{aligned} \tag{1.149}$$

where we are integrating over periodic trajectories; therefore, the boundary conditions are (later, we will use different boundary conditions for the double-well potential)

$$r(-\beta/2) = r(\beta/2), \quad \dot{r}(-\beta/2) = \dot{r}(\beta/2). \tag{1.150}$$

We need to perform the Gaussian integration over $r(t)$. In order to do that, we introduce a complete set of orthonormal eigenfunctions $x_n(\tau)$ of $\mathbf{M}$ (orthonormal set exists because it is a Hermitian operator, its completeness in $L^2(-\beta/2, \beta/2)$ is discussed in [10])

$$\mathbf{M}x_n = \lambda_n x_n, \quad n = 0, 1, \ldots, \tag{1.151}$$

$$\left[-\left(\frac{\mathrm{d}}{\mathrm{d}\tau}\right)^2 + V''(x_{\mathrm{in}}^{\tau_0}(\tau))\right] x_n(\tau) = \lambda_n x_n(\tau), \quad n = 0, 1, \ldots, \tag{1.152}$$

which satisfy the same boundary conditions as $r(t)$. By orthonormality we mean

$$\int_{-\beta/2}^{\beta/2} \mathrm{d}\tau\, x_n(\tau) x_m(\tau) = \delta_{nm}, \tag{1.153}$$

where we assume we have a discrete spectrum. This is not the case in many cases, but the formalism developed with this assumption can be easily generalized. We will use an orthonormal set of eigenfunctions to expand the fluctuations

$$r(\tau) = \sum_{n\geq 0} c_n x_n(\tau)\,, c_n \in \mathbb{R}. \tag{1.154}$$

This can be understood as a change of variables from the set of paths $r(\tau)$ to coefficients c_n. All possible configurations of the system are parametrized by these coefficients. Therefore the measure for $r(\tau)$ is defined as

$$\mathcal{D}r(\tau) = \mathcal{N} \prod_{n\geq 0} \frac{\mathrm{d}c_n}{\sqrt{2\pi}}, \tag{1.155}$$

and we can rewrite the expression for the path integral

$$\begin{aligned} &\int_{r(-\beta/2)=r(\beta/2)} \mathcal{D}r(\tau)\, \exp\left(-\frac{1}{2}\int_{-\beta/2}^{\beta/2} \mathrm{d}\tau_1 \mathrm{d}\tau_2\, r(\tau_1) M(\tau_1, \tau_2) r(\tau_2)\right) = \\ &= \mathcal{N} \int \prod_{n\geq 0} \frac{\mathrm{d}c_n}{\sqrt{2\pi}}\, \exp\left(-\frac{1}{2}\sum_{n\geq 0} \lambda_n c_n^2\right) = \mathcal{N}(\det \mathbf{M})^{-1/2}, \end{aligned} \tag{1.156}$$

where

$$\det \mathbf{M} = \prod_{n\geq 0} \lambda_n. \tag{1.157}$$

Our new task is calculating the determinant of $\mathbf{M}$. This looks straightforward, but there are many subtleties to be taken into account.

Firstly, we will take the time derivative of the Euclidean equation of motion (remember, we are working with the potential (1.141))

$$\ddot{x}_{\text{in}}^{\tau_0}(\tau) - V'(x_{\text{in}}^{\tau_0}(\tau)) = 0,$$
$$\frac{\mathrm{d}^2}{\mathrm{d}\tau^2}\dot{x}_{\text{in}}^{\tau_0}(\tau) - V''(x_{\text{in}}^{\tau_0}(\tau))\dot{x}_{\text{in}}^{\tau_0}(\tau) = 0.$$

Instanton $x_{\text{in}}^{\tau_0}(\tau)$ for the potential (1.141) is periodic (the periodic boundary conditions), therefore $\dot{x}_{\text{in}}^{\tau_0}(\tau)$ also satisfies the periodic boundary conditions. That means that $\dot{x}_{\text{in}}^{\tau_0}(\tau)$ is a zero mode of $\mathbf{M}$, which means eigenfunction with zero eigenvalue. After normalization, it has to be one of the eigenfunctions, for example

$$x_1(\tau) = \frac{\dot{x}_{\text{in}}^{\tau_0}(\tau)}{\|\dot{x}_{\text{in}}^{\tau_0}\|}, \tag{1.158}$$

where the norm is

$$\|\dot{x}_{\text{in}}^{\tau_0}\|^2 = \int_{-\beta/2}^{\beta/2} \mathrm{d}\tau (\dot{x}_{\text{in}}^{\tau_0}(\tau))^2 = \mathcal{W}(E). \tag{1.159}$$

We have to address the issue of the existence of the zero mode. Naively, one suspects that the determinant vanishes and expression for the path integral explodes. A closer look is needed. The explosion of the expression for the path integral is due to the absence of a damping exponential factor for c_1. We will isolate this apparent divergence

$$\int \prod_{n\geq 0} \frac{\mathrm{d}c_n}{\sqrt{2\pi}} \exp\left(-\frac{1}{2}\sum_{n\geq 0}\lambda_n c_n^2\right) = \left(\int \frac{\mathrm{d}c_1}{\sqrt{2\pi}}\right)(\det{}' \mathbf{M})^{-1/2}, \tag{1.160}$$

where

$$\det{}' \mathbf{M} = \prod_{n\neq 1} \lambda_n. \tag{1.161}$$

We must be cautious with integrating over c_1 since this variable stands for collective coordinate τ_0, as shown in the following. The coefficient c_1 was introduced in the expansion of arbitrary periodic function $r(\tau)$ in (1.154) however we could also expand such a function as

$$r(\tau) = x_{\text{in}}^{\tau_0}(\tau) + \sum_{n\neq 1} c_n x_n(\tau), \tag{1.162}$$

where collective coordinate τ_0 is now understood as a coordinate in the space of configurations. Indeed, if we vary c_1 in (1.154), we get

$$\delta r(\tau) = x_1(\tau)\delta c_1 = \frac{\dot{x}_{\text{in}}^{\tau_0}(\tau)}{\|\dot{x}_{\text{in}}^{\tau_0}\|}\delta c_1, \tag{1.163}$$

while varying τ_0 in (1.162) gives

$$\delta r(\tau) = -\dot{x}_{\text{in}}^{\tau_0}(\tau)\delta\tau_0. \tag{1.164}$$

We can see that both variations are proportional, and τ_0 parametrizes the same fluctuations as c_1. Jacobian of this change of variables is

$$J = \left|\frac{\delta c_1}{\delta \tau_0}\right| = \|\dot{x}_{\text{in}}^{\tau_0}\| = \sqrt{\mathcal{W}(E)}. \tag{1.165}$$

Therefore, the integration over c_1 gives

$$\frac{1}{\sqrt{2\pi}}\int \mathrm{d}c_1 = \frac{J}{\sqrt{2\pi}}\int_{-\beta/2}^{\beta/2}\mathrm{d}\tau_0 = \frac{\beta\sqrt{\mathcal{W}(E)}}{\sqrt{2\pi}}, \tag{1.166}$$

where we used that $\tau_0 \in [-\beta/2, \beta/2]$.

There is one more important property of the operator $\mathbf{M}$ – it has one and only one negative mode. This can be seen regarding the operator $\mathbf{M}$ as a one-dimensional Schrödinger operator (we mean the operator of a one-dimensional time-independent Schrödinger equation) after formal substitution $\tau \to x$. We can use the Node theorem (intuitive proof in [11]), which says that for the one-dimensional Schrödinger equation, the wavefunction of n-th bound state has $n-1$ nodes (zeros). We know that $\dot{x}_{\text{in}}^{\tau_0}$ changes sign once (from one turning point to the other and back); therefore, there must be an eigenfunction with a lower eigenvalue. Since the eigenvalue of x_1 is zero, the eigenvalue of x_0 is negative; this is the only negative mode of $\mathbf{M}$.

This means we would like to understand what is going on with the integral

$$\int \frac{\mathrm{d}c_0}{\sqrt{2\pi}}\,\exp\left(-\frac{1}{2}\lambda_0 c_0^2\right), \tag{1.167}$$

when $\lambda_0 < 0$. We will again use the analytic continuation. We take λ_0 and c_0 to be generally complex. The integral is convergent if

$$\mathrm{Re}(\lambda_0 c_0^2) > 0 \quad \Rightarrow \quad \mathrm{Arg}(c_0) = -\frac{1}{2}\mathrm{Arg}(\lambda_0). \tag{1.168}$$

To make λ_0 complex and maintain convergence, we must rotate the integration contour. When $\lambda_0 = -|\lambda_0| \pm i0$, then $\mathrm{Arg}\, c_0 = \mp\pi/2$ as depicted in Figure 1.14 and the result of the integral is $\mp i|\lambda_0|^{-1/2}$.

The sign ambiguity is related to the sign ambiguity in equation (1.144) (see [12]). We choose the branch cut so that the final result is positive. In the following, we will see why is this choice convenient.

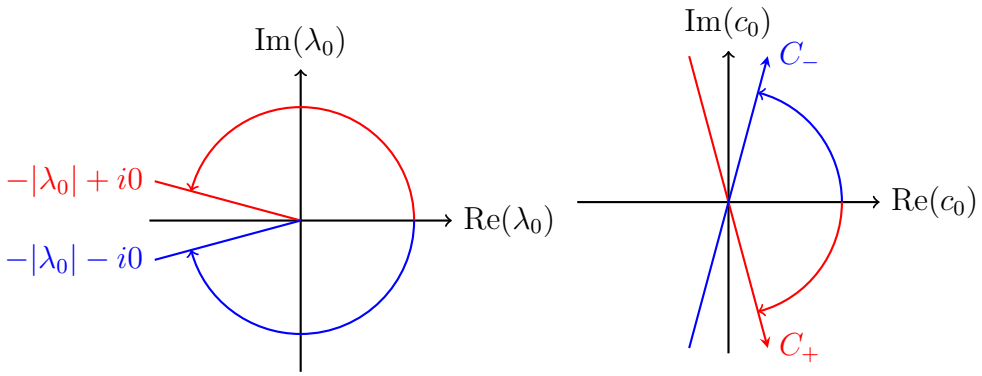

Figure 1.14: As we are approaching negative λ_0 from above and below we must rotate integration contour C_+ to $-\pi/2$ and C_- to $\pi/2$.

Putting it all together, we get

$$\mathrm{Im}(Z(\beta)) \approx \frac{1}{2i}\exp(-S_{\mathrm{in}})\mathcal{N}\frac{\beta\sqrt{\mathcal{W}(E)}}{\sqrt{2\pi}}(\det{}'\,\mathbf{M})^{-1/2}. \tag{1.169}$$

We have to get rid of $\mathcal{N}$. To do that, we use the known partition function for the harmonic oscillator (with $\omega = 1$)

$$Z_0(\beta) = \mathcal{N}(\det\mathbf{M}_0)^{-1/2} = \frac{1}{2\sinh(\beta/2)}, \tag{1.170}$$

$$\mathbf{M}_0 = -\frac{\mathrm{d}^2}{\mathrm{d}\tau^2} + 1. \tag{1.171}$$

It follows that

$$\mathrm{Im}(Z(\beta)) \approx \frac{1}{2i}\exp(-S_{\mathrm{in}})Z_0(\beta)\frac{\beta\sqrt{\mathcal{W}(E)}}{\sqrt{2\pi}}\left(\frac{\det{}'\,\mathbf{M}}{\det\mathbf{M}_0}\right)^{-1/2}. \tag{1.172}$$

From the start, we assumed that we had perturbed a quadratic potential; therefore, in the limit of $g \to 0$, we expect the partition function of the harmonic oscillator, which is real. The partition function has also the real part. We got only the imaginary one because we were calculating the path integral around the instanton which is the nontrivial solution to the Euclidean equation of motion. If we were calculating the path integral around a constant solution (which, in this case, satisfies periodic boundary conditions) in the one-loop approximation, we would get the real part of the partition function

$$\mathrm{Re}(Z(\beta)) \approx Z_0(\beta). \tag{1.173}$$

Let us use results (1.172) and (1.173) to derive one more result – the imaginary part of the ground state energy. We will use the Helmholtz free energy and $\beta \to \infty$ limit

$$F(\beta) = -\frac{1}{\beta}\ln(Z(\beta)) = -\frac{1}{\beta}\ln\left[\sum_{n=0}^{\infty}\exp(-\beta E_n)\right], \tag{1.174}$$

$$E_0 = \lim_{\beta\to\infty} F(\beta). \tag{1.175}$$

Now we will use an expansion in powers of $\mathrm{Im}(Z(\beta))$ (it is small for $g \to 0$)

$$\begin{aligned} F(\beta) &= -\frac{1}{\beta}\ln(Z(\beta)) = -\frac{1}{\beta}\ln[\mathrm{Re}(Z(\beta)) + i\mathrm{Im}(Z(\beta))] = \\ &= -\frac{1}{\beta}\ln[\mathrm{Re}(Z(\beta))] - \frac{1}{\beta}\ln\left[1 + i\frac{\mathrm{Im}(Z(\beta))}{\mathrm{Re}(Z(\beta))}\right] \approx \\ &\approx -\frac{1}{\beta}\left\{\ln[\mathrm{Re}(Z(\beta))] + i\frac{\mathrm{Im}(Z(\beta))}{\mathrm{Re}(Z(\beta))}\right\}, \\ \mathrm{Im}(F(\beta)) &\approx -\frac{1}{\beta}\frac{\mathrm{Im}(Z(\beta))}{\mathrm{Re}(Z(\beta))}. \end{aligned} \tag{1.176}$$

Thus, we have

$$\mathrm{Im}(E_0) = \lim_{\beta\to\infty}\mathrm{Im}(F(\beta)) = -\lim_{\beta\to\infty}\frac{1}{\beta}\frac{\mathrm{Im}(Z(\beta))}{\mathrm{Re}(Z(\beta))}. \tag{1.177}$$

Using equations (1.140), (1.172) and (1.173), we get the imaginary part of the ground state energy

$$\mathrm{Im}(E_0) \approx -\frac{1}{2i}\exp(-S_{\mathrm{in}})\frac{\sqrt{S_{\mathrm{in}}}}{\sqrt{2\pi}}\lim_{\beta\to\infty}\left(\frac{\det'\mathbf{M}}{\det\mathbf{M}_0}\right)^{-1/2}. \tag{1.178}$$

Now we can see why we chose the imaginary part of the partition function to be positive. We did so because that way the imaginary part for the ground state of the unstable potential is negative; which is consistent with equation (1.127).

The quotient of the determinant of $\mathbf{M}$ by the reference determinant of $\mathbf{M}_0$ is essential. The eigenvalues of Schrödinger operators of the type (1.148) grow as $\lambda_n \approx n^2$ for $n \gg 1$ (see [4]). Therefore, with the quotient of these two determinants, we expect that divergent parts will cancel out, and we will be left with something finite. The following section will explain how to calculate the determinants of some valuable operators.

1.2.4 Pöschl–Teller operators

We will investigate the family of operators called Pöschl-Teller operators

$$\mathbf{M}_{l,m} = -\frac{\mathrm{d}^2}{\mathrm{d}x^2} + m^2 - \frac{l(l+1)}{\cosh^2 x}, \tag{1.179}$$

where $l, m \in \mathbb{N} \cup \{0\}$ are parameters. These operators can be understood as Schrödinger operators in an inverted $\cosh^2$ potential, also called Pöschl-Teller potential. The spectrum of these operators can be determined exactly. Let us introduce the operators

$$A_l = \frac{\mathrm{d}}{\mathrm{d}x} + l\tanh x, \tag{1.180}$$

$$A_l^\dagger = -\frac{\mathrm{d}}{\mathrm{d}x} + l\tanh x. \tag{1.181}$$

It follows that

$$A_l^\dagger A_l = \mathbf{M}_{l,m} + l^2 - m^2, \tag{1.182}$$
$$A_l A_l^\dagger = \mathbf{M}_{l-1,m} + l^2 - m^2. \tag{1.183}$$

Let us introduce the interesting properties of these operators. We will take advantage of the fact that if $\psi^{(l)}(x)$ is an eigenfunction of $\mathbf{M}_{l,m}$ with eigenvalue μ_l, then

$$\psi^{(l-1)}(x) = A_l \psi^{(l)}(x) \tag{1.184}$$

is an eigenfunction of $\mathbf{M}_{l-1,m}$ with the same eigenvalue

$$\begin{aligned}
&\mathbf{M}_{l-1,m}\psi^{(l-1)}(x) = (A_l A_l^\dagger - l^2 + m^2) A_l \psi^{(l)}(x) = \\
&= A_l(\mathbf{M}_{l,m} + l^2 - m^2)\psi^{(l)}(x) + (m^2 - l^2)\psi^{(l-1)}(x) = \\
&= (\mu_l + l^2 - m^2)\psi^{(l-1)}(x) + (m^2 - l^2)\psi^{(l-1)}(x) = \\
&= \mu_l \psi^{(l-1)}(x).
\end{aligned} \tag{1.185}$$

We can easily find a ground state of the operator $\mathbf{M}_{l,m}$ by solving

$$A_l \psi_0^{(l)}(x) = 0. \tag{1.186}$$

The solution to this first-order differential equation is

$$\psi_0^{(l)}(x) \propto \frac{1}{\cosh^l(x)}. \tag{1.187}$$

Using the operator from (1.182) on this function we get

$$\begin{aligned}
&A_l^\dagger A_l \psi_0^{(l)}(x) = \mathbf{M}_{l,m}\psi_0^{(l)}(x) + (l^2 - m^2)\psi_0^{(l)}(x), \\
&0 = \mathbf{M}_{l,m}\psi_0^{(l)}(x) + (l^2 - m^2)\psi_0^{(l)}(x), \\
&\mathbf{M}_{l,m}\psi_0^{(l)}(x) = (m^2 - l^2)\psi_0^{(l)}(x).
\end{aligned} \tag{1.188}$$

Therefore, the ground-state energy is

$$E_0^{(l,m)} = m^2 - l^2. \tag{1.189}$$

Let us proceed to calculate excited states. This time, we will take advantage of the fact that if $\psi^{(l-1)}(x)$ is an eigenfunction of $\mathbf{M}_{l-1,m}$ with eigenvalue μ_{l-1}, then

$$\psi^{(l)}(x) = A_l^\dagger \psi^{(l-1)}(x) \tag{1.190}$$

is an eigenfunction of $\mathbf{M}_{l,m}$ with the same eigenvalue

$$\begin{aligned}
&\mathbf{M}_{l,m}\psi^{(l)}(x) = (A_l^\dagger A_l - l^2 + m^2) A_l^\dagger \psi^{(l-1)}(x) = \\
&= A_l^\dagger(\mathbf{M}_{l-1,m} + l^2 - m^2)\psi^{(l-1)}(x) + (m^2 - l^2)\psi^{(l)}(x) = \\
&= (\mu_{l-1} + l^2 - m^2)\psi^{(l)}(x) + (m^2 - l^2)\psi^{(l)}(x) = \\
&= \mu_{l-1}\psi^{(l)}(x).
\end{aligned} \tag{1.191}$$

We will build the spectrum of $\mathbf{M}_{l,m}$ starting with the $l = 0$ state and applying the $A_l^\dagger$ operator. For $l = 0$, we get a free particle (in the sense of the particle in Pöschl-Teller potential), and the eigenfunctions are plane waves (so-called scattering states)

$$\psi^{(0)}(k, x) \propto \exp(ikx) \tag{1.192}$$

with energies

$$E^{(0,m)}(k) = k^2 + m^2. \tag{1.193}$$

Applying operator $A_1^\dagger$ on scattering states above, we get scattering states for $l = 1$

$$\psi^{(1)}(k, x) \propto A_1^\dagger \exp(ikx), \tag{1.194}$$

and we have the ground state

$$\psi_0^{(1)}(x) \propto \frac{1}{\cosh(x)}. \tag{1.195}$$

Again, by applying operator $A_2^\dagger$ on scattering states above, we get scattering states for $l = 2$

$$\psi^{(2)}(k, x) \propto A_2^\dagger A_1^\dagger \exp(ikx). \tag{1.196}$$

Also, we have the bound state

$$\psi_1^{(2)}(x) \propto A_2^\dagger \frac{1}{\cosh(x)}, \tag{1.197}$$

and the new ground state

$$\psi_0^{(2)}(x) \propto \frac{1}{\cosh^2(x)}. \tag{1.198}$$

Iterating this way, we obtain the full spectrum of l-th potential. It consists of scattering states

$$\psi^{(l)}(k, x) \propto A_l^\dagger \dots A_1^\dagger \exp(ikx) \tag{1.199}$$

with energies

$$E^{(l,m)}(k) = k^2 + m^2, \tag{1.200}$$

and l bound states

$$\psi_0^{(l)}(x) \propto \frac{1}{\cosh^l(x)}, \tag{1.201}$$

$$\psi_j^{(l)}(x) \propto A_l^\dagger \dots A_{l-j+1}^\dagger \frac{1}{\cosh^{l-j}(x)}, \quad j = 1, \dots, l-1, \tag{1.202}$$

with energies

$$E_j^{(l,m)} = m^2 - (l-j)^2, \quad j = 0, \dots, l-1. \tag{1.203}$$

This can be seen from the fact that eigenvalue of j-th state in l-th potential is same as eigenvalue of $(j-1)$-th state in $(l-1)$-th potential

$$\begin{aligned}
&\mathbf{M}_{l,m}\psi_j^{(l)}(x) = (A_l^\dagger A_l - l^2 + m^2)\psi_j^{(l)}(x) = \\
&= A_l^\dagger A_l A_l^\dagger \dots A_{l-j+1}^\dagger \frac{1}{\cosh^{l-j}(x)} + (m^2 - l^2)\psi_j^{(l)}(x) = \\
&= A_l^\dagger (\mathbf{M}_{l-1,m} + l^2 - m^2) A_{l-1}^\dagger \dots A_{l-j+1}^\dagger \frac{1}{\cosh^{l-j}(x)} + (m^2 - l^2)\psi_j^{(l)}(x) = \\
&= A_l^\dagger \mathbf{M}_{l-1,m} A_{l-1}^\dagger \dots A_{(l-1)-(j-1)+1}^\dagger \frac{1}{\cosh^{(l-1)-(j-1)}(x)} = \\
&= A_l^\dagger \mathbf{M}_{l-1,m} \psi_{j-1}^{(l-1)}(x) = E_{j-1}^{(l-1,m)} \psi_j^{(l)}(x).
\end{aligned} \tag{1.204}$$

Now that we know the full spectrum of the operator $\mathbf{M}_{l,m}$, we can calculate its determinant. As a reference determinant, we will take again the harmonic oscillator operator $\mathbf{M}_{0,m}$, which corresponds to the free particle in the context of Pöschl-Teller potentials. As we have seen, eigenfunctions of $\mathbf{M}_{l,m}$ consist of scattering and bound states, which means that the spectrum will have discrete part $\{\lambda_n\}$ and continuous part $\lambda(k)$. Determinant should be understood as

$$\log(\det \mathbf{M}_{l,m}) = \sum_n \log(\lambda_n) + \int \mathrm{d}k\, \rho(k) \log(\lambda(k)), \tag{1.205}$$

where $\rho(k)$ is the density of states for the continuous part. To calculate $\rho(k)$, we will work in a large box of length $L \to \infty$. As $x \to \pm\infty$ we have

$$A_j^\dagger \approx -\frac{\mathrm{d}}{\mathrm{d}x} \pm j, \tag{1.206}$$

and scattering states will be

$$\psi^{(l)}(k,x) \approx \prod_{j=1}^{l} (-ik \pm j) \exp(ikx), \quad x \to \pm\infty. \tag{1.207}$$

This can be rewritten as (up to normalization – we are interested in the phase)

$$\psi^{(l)}(k,x) \approx \exp\left(ikx \pm i\frac{\theta(k)}{2}\right), \tag{1.208}$$

where (small exercise for the reader)

$$\frac{\theta(k)}{2} = -\sum_{j=1}^{l} \arctan\left(\frac{k}{j}\right). \tag{1.209}$$

We will use the large-box quantization

$$\begin{aligned}
&\psi_+^{(l)}(k, x+L) = \psi_-^{(l)}(k,x), \\
&kL + \theta(k) = 2\pi n,\ n \in \mathbb{N} \cup \{0\},
\end{aligned} \tag{1.210}$$

and get the density of states as

$$\rho(k) = \frac{\mathrm{d}n}{\mathrm{d}k} = \frac{L}{2\pi} + \frac{\theta'(k)}{2\pi} = \rho_{\text{free}}(k) + \rho_\theta(k), \tag{1.211}$$

where

$$\rho_\theta(k) = -\frac{1}{\pi}\sum_{j=1}^{l} \frac{j}{j^2+k^2}. \tag{1.212}$$

Using all derived results, we can get back to calculating the quotient of our two determinants

$$\begin{aligned}
&\log\left(\frac{\det' \mathbf{M}_{l,m}}{\det \mathbf{M}_{0,m}}\right) = \log(\det' \mathbf{M}_{l,m}) - \log(\det \mathbf{M}_{0,m}) = \\
&= \sum_{1\le j\le l,\, j\neq m} \log(m^2-j^2) + \int_{-\infty}^{\infty} \mathrm{d}k\, (\rho_{\text{free}}(k) + \rho_\theta(k)) \log(k^2+m^2) - \\
&- \int_{-\infty}^{\infty} \mathrm{d}k\, \rho_{\text{free}}(k) \log(k^2+m^2) = \\
&= \sum_{1\le j\le l,\, j\neq m} \log(m^2-j^2) - \frac{1}{\pi}\sum_{j=1}^{l} j \int_{-\infty}^{\infty} \frac{\mathrm{d}k}{k^2+j^2}\, \log(k^2+m^2) = \\
&= \sum_{1\le j\le l,\, j\neq m} \log(m^2-j^2) - \frac{1}{\pi}\sum_{j=1}^{l} j \left(\frac{2\pi}{j}\log(j+m)\right) = \\
&= \sum_{1\le j\le l,\, j\neq m} \log(m^2-j^2) - 2\sum_{j=1}^{l} \log(j+m) = \\
&= \log\left[\frac{\prod_{1\le j\le l,\, j\neq m}(m^2-j^2)}{\prod_{1\le j\le l}(m+j)^2}\right].
\end{aligned} \tag{1.213}$$

Thus, the result for the quotient of our determinants for $l \geq 1$ is

$$\boxed{\frac{\det' \mathbf{M}_{l,m}}{\det \mathbf{M}_{0,m}} = \frac{\prod_{1\le j\le l,\, j\neq m}(m^2-j^2)}{\prod_{1\le j\le l}(m+j)^2},} \tag{1.214}$$

for $(l,m) \neq (1,1)$. For $l = m = 1$, the numerator should be taken as 1 since there is no contribution from discrete states.

At the end, we will look at the effect on the quotient of determinants caused by rescaling operators for $m \leq l$. Let us suppose that we rescale by a factor ξ

$$\mathbf{M}_{l,m} \to \xi \mathbf{M}_{l,m}, \quad \mathbf{M}_{0,m} \to \xi \mathbf{M}_{0,m}. \tag{1.215}$$

This rescaling results into

$$\frac{\det' \mathbf{M}_{l,m}}{\det \mathbf{M}_{0,m}} \to \xi^{N'_{l,m} - N_{0,m}} \frac{\det' \mathbf{M}_{l,m}}{\det \mathbf{M}_{0,m}}, \tag{1.216}$$

where $N'_{l,m} - N_{0,m}$ is difference between number of nonzero modes of $\mathbf{M}_{l,m}$ and number of modes of $\mathbf{M}_{0,m}$. That can be easily calculated

$$\begin{aligned} N'_{l,m} - N_{0,m} &= (l-1) + \int_{-\infty}^{\infty} \mathrm{d}k\, \rho_\theta(k) = \\ &= (l-1) - \frac{1}{\pi} \sum_{j=1}^{l} j \int_{-\infty}^{\infty} \frac{\mathrm{d}k}{k^2 + j^2} = (l-1) - l = -1. \end{aligned} \tag{1.217}$$

Thus, after rescaling, we get

$$\frac{\det' \mathbf{M}_{l,m}}{\det \mathbf{M}_{0,m}} \to \frac{1}{\xi} \frac{\det' \mathbf{M}_{l,m}}{\det \mathbf{M}_{0,m}}. \tag{1.218}$$

1.2.5 Instantons in the double-well potential

We will use all the things we have developed to calculate the splitting of the ground-state energy in the double-well potential. We will be working with the potential from (1.132), which is

$$V(x) = \frac{g}{2} \left(x^2 - \frac{1}{4g} \right)^2, \; g > 0. \tag{1.219}$$

The Hamiltonian is invariant under $x \to -x$, which means that it commutes with parity operator $\hat{P}$. The action of the parity operator is

$$\hat{P}\psi(x) = \psi(-x). \tag{1.220}$$

Since $\hat{P}$ commutes with the Hamiltonian $\hat{H}$ they can be simultaneously diagonalized

$$\hat{H}\psi_{\epsilon,n}(x) = E_{\epsilon,n}\psi_{\epsilon,n}(x), \tag{1.221}$$

$$\hat{P}\psi_{\epsilon,n}(x) = \epsilon\psi_{\epsilon,n}(x), \tag{1.222}$$

where $\epsilon = \pm 1$ is the parity. By the quantum number $n \in \mathbb{N} \cup \{0\}$, we mean that in the limit of small coupling constant $g \to 0$, we have

$$E_{\epsilon,n} = n + \frac{1}{2} + \mathcal{O}(g). \tag{1.223}$$

As mentioned, the energy difference of the first excited and the ground state $E_{-,0} - E_{+,0}$ is invisible by perturbative methods and has classical instanton dependence. We must find a quantity that can be calculated with the path integral and expressed via the energy difference. The canonical partition function can be expressed via the path integral but does not give us the energy difference. However, we can consider the twisted partition function

$$Z_{\mathrm{t}}(\beta) = \mathrm{Tr}[\hat{P} \exp(-\beta \hat{H})], \tag{1.224}$$

where $\hat{P}$ is the already mentioned parity operator. In the limit $\beta \to \infty$ and small coupling constant $g \to 0$ we can write for the twisted partition function

$$\begin{aligned} Z_{\mathrm{t}}(\beta) &\approx \exp(-\beta E_{+,0}) - \exp(-\beta E_{-,0}) = \\ &= \exp(-\beta E_{+,0})\{1 - \exp[-\beta(E_{-,0} - E_{+,0})]\} \approx \\ &\approx \beta \exp(-\beta/2)(E_{-,0} - E_{+,0}). \end{aligned} \tag{1.225}$$

Also, it can be expressed via path integral with twisted boundary conditions

$$Z_{\mathrm{t}}(\beta) = \int_{x(\beta/2)=\hat{P}x(-\beta/2)} \mathcal{D}x(\tau)\, \exp\left(-S_{\mathrm{E}}[x(\tau)]\right), \tag{1.226}$$

therefore boundary conditions are $x(\beta/2) = -x(-\beta/2)$. In expression (1.136), we have seen the instanton and the anti-instanton solutions for a particle in the double-well potential in the $\beta \to \infty$ limit

$$x_{\mathrm{in}}^{\tau_0}(\tau) = \pm\frac{1}{2\sqrt{g}} \tanh\left(\frac{\tau-\tau_0}{2}\right), \tag{1.227}$$

which satisfied these boundary conditions. The operator $\mathbf{M}$ from (1.148) takes the form

$$\mathbf{M} = -\frac{\mathrm{d}^2}{\mathrm{d}\tau^2} + 1 - \frac{3}{2\cosh^2\left(\frac{\tau-\tau_0}{2}\right)}, \tag{1.228}$$

which is proportional to the Pöschl-Teller operator $\mathbf{M}_{2,2}$

$$\mathbf{M} = \frac{1}{4}\mathbf{M}_{2,2}, \tag{1.229}$$

after rescaling time $\tau \to 2\tau$ in the operator $\mathbf{M}$. From the spectrum of the Pöschl-Teller operators (1.203), we know that the operator $\mathbf{M}$ has one zero mode and no negative mode. This agrees with the fact that we are studying the stable potential. Similarly, as for the canonical partition function, we can perform a one-loop approximation of path integral for the twisted partition function. The steps of derivation are the same as for the canonical partition function (now it is easier because the path integral expression for the twisted partition function is well defined and it has just the real part), and we get

$$Z_{\mathrm{t}}(\beta) \approx 2\exp(-S_{\mathrm{in}}) Z_0(\beta) \frac{\beta\sqrt{S_{\mathrm{in}}}}{\sqrt{2\pi}} \left(\frac{\det' \mathbf{M}}{\det \mathbf{M}_0}\right)^{-1/2}, \tag{1.230}$$

where factor two is because the instanton and the anti-instanton give the same contribution, and we used the fact that in the limit $\beta \to \infty$, $\mathcal{W}(0) = S_{\mathrm{in}}$. This time, the constant solution to the Euclidean equation of motion does not satisfy boundary conditions. Using equation (1.225) we can write expression for the energy splitting

$$E_{-,0} - E_{+,0} \approx 2\frac{\sqrt{S_{\mathrm{in}}}}{\sqrt{2\pi}} \exp(-S_{\mathrm{in}}) \left(\frac{\det' \mathbf{M}}{\det \mathbf{M}_0}\right)^{-1/2}, \tag{1.231}$$

where we used expression (1.170) for Z_0. Action for the instanton and anti-instanton trajectory in $\beta \to \infty$ limit ($E = 0$) is

$$\begin{aligned} S_{\text{in}} = \mathcal{W}(0) &= \int_{-\beta/2}^{\beta/2} \mathrm{d}\tau (\dot{x}_{\text{in}}^{\tau_0}(\tau))^2 = \\ &= 2\int_0^{\frac{1}{2\sqrt{g}}} p_{\text{in}}(x)\,\mathrm{d}x = 2\int_0^{\frac{1}{2\sqrt{g}}} \sqrt{2V(x)}\,\mathrm{d}x = \\ &= 2\int_0^{\frac{1}{2\sqrt{g}}} \sqrt{g\left(x^2 - \frac{1}{4g}\right)^2}\,\mathrm{d}x = \\ &= 2\sqrt{g}\int_0^{\frac{1}{2\sqrt{g}}} \left|x^2 - \frac{1}{4g}\right|\,\mathrm{d}x = \\ &= 2\sqrt{g}\left[\left|\frac{x^3}{3} - \frac{x}{4g}\right|\right]_0^{\frac{1}{2\sqrt{g}}} = \frac{1}{6g}. \end{aligned} \tag{1.232}$$

For calculating the quotient of determinants we use equations (1.216), (1.218), (1.229) and we have

$$\frac{\det' \mathbf{M}}{\det \mathbf{M}_0} = 4\frac{\det' \mathbf{M}_{2,2}}{\det \mathbf{M}_{0,2}} = 4\frac{4-1}{(2+1)^2(2+2)^2} = \frac{1}{12}. \tag{1.233}$$

Putting it all together, we get the final expression for the splitting of the ground-state energy

$$\Delta E = E_{-,0} - E_{+,0} \approx \frac{2}{\sqrt{\pi g}} \exp\left(-\frac{1}{6g}\right), \tag{1.234}$$

which is in agreement with the result obtained by the WKB method in (1.103) after substitution $\lambda = \frac{1}{2\sqrt{g}}$, $\hbar = \omega = m = 1$. This time, the parameter describing the energy splitting is g. The splitting of the ground state energy is exponentially suppressed in the small g limit.

Better results for the ground-state energy splitting can be obtained by the n-loop approximations. The idea behind the n-loop approximation is to integrate not just over quadratic fluctuations $S_{(2)}$ giving us the Gaussian integral, but also over higher-order fluctuations from the expression

$$\begin{aligned} &\int \mathcal{D}x(\tau)\, \exp(-S_{\text{E}}[x(\tau)]) = \\ &= \exp(-S_{\text{in}}) \int \mathcal{D}x(\tau)\, \exp[-(S_{(2)} + S_{(3)} + S_{(4)} + \ldots)]. \end{aligned} \tag{1.235}$$

These higher-order fluctuations give us the result in the form

$$\Delta E \approx \frac{2}{\sqrt{\pi g}} \exp\left(-\frac{1}{6g}\right)(a_0 + g a_1 + g^2 a_2 + g^3 a_3 + \ldots + g^{n-1} a_{n-1}), \tag{1.236}$$

where we found out that $a_0 = 1$ which is the one-loop approximation. In [6] Kleinert found out that $a_2 = -\frac{71}{12}$, which is the two-loop approximation, and in [13] Escobar-Ruiz, Shuryak and Turbiner found out that $a_3 \approx 21.8713$, which is the three-loop approximation. The name of the approximation comes from the fact that higher coefficients are calculated via many-loop Feynman diagrams.

2. Bootstrapping quantum mechanics

In this chapter, we will introduce a numerical method for calculating energy levels for a given type of potential. The method is called bootstrap, which, according to Oxford Learner's Dictionaries, literally means an approach to creating something that uses the minimum amount of resources possible. This is precisely how we will proceed, using just symmetry and three basic identities. Following the steps of [14] and [15], we will use the first two identities to derive a recursive relation for the moments $\langle x^n \rangle$. The third identity will decide if the resulting moment sequence is accepted or rejected. Since energy and a few other parameters are data to start the recursion, this gives us bounds on acceptable energies. Then, we will go through the algorithmic structure of the method itself. Finally, we will briefly look at using the bootstrap in single-matrix quantum mechanics as was done in [1].

2.1 The recursion relation

We will derive the three basic identities, which are the three pillars on which the method holds. Let us denote eigenstates of the Hamiltonian $\hat{H}$ with eigenvalues E as $|E\rangle$. It follows for any operator $\hat{O}$ that

$$\langle E|[\hat{H},\hat{O}]|E\rangle = \langle E|(\hat{H}\hat{O}-\hat{O}\hat{H})|E\rangle = E\langle E|\hat{O}|E\rangle - E\langle E|\hat{O}|E\rangle = 0, \quad (2.1)$$

$$\langle E|\hat{H}\hat{O}|E\rangle = E\langle E|\hat{O}|E\rangle, \quad (2.2)$$

$$\langle E|\hat{O}^\dagger\hat{O}|E\rangle = (\hat{O}|E\rangle)^\dagger(\hat{O}|E\rangle) \geq 0. \quad (2.3)$$

We will be working in the one-dimensional quantum mechanics with the Hamiltonian

$$\hat{H} = \frac{\hat{p}^2}{2M} + V(\hat{x}), \quad (2.4)$$

where $\hat{x} = x$ and $\hat{p} = -i\hbar\frac{\mathrm{d}}{\mathrm{d}x}$ are x-representations of coordinate and momentum operators and M is mass of a particle. Now we will use identities (2.1) and (2.2) for special operators $\hat{O}$. We will start with $\hat{O} = \hat{x}^n$, where $n \in \mathbb{N}\cup\{0\}$. Setting $\hbar = 1$, $M = 1$ and using identity (2.1) we see that

$$\begin{aligned} 0 &= \langle E|\left[\frac{1}{2}\hat{p}^2 + V(\hat{x}), \hat{x}^n\right]|E\rangle = \langle E|\left(\frac{1}{2}\hat{p}^2\hat{x}^n - \frac{1}{2}\hat{x}^n\hat{p}^2\right)|E\rangle = \\ &= \langle E|\left[\frac{1}{2}\hat{x}^n\hat{p}^2 - in\hat{x}^{n-1}\hat{p} - \frac{1}{2}n(n-1)\hat{x}^{n-2} - \frac{1}{2}\hat{x}^n\hat{p}^2\right]|E\rangle = \\ &= \langle E|\left[-in\hat{x}^{n-1}\hat{p} - \frac{1}{2}n(n-1)\hat{x}^{n-2}\right]|E\rangle. \end{aligned} \quad (2.5)$$

Using (2.1) and (2.2) we see that

$$\langle E|\hat{x}^n\left(\frac{\hat{p}^2}{2} + V(\hat{x})\right)|E\rangle = E\langle E|\hat{x}^n|E\rangle. \quad (2.6)$$

Therefore, in simplified notation, we get

$$n\langle x^{n-1}p\rangle = \frac{i}{2}n(n-1)\langle x^{n-2}\rangle, \tag{2.7}$$

$$\frac{1}{2}\langle x^n p^2\rangle + \langle x^n V(x)\rangle = E\langle x^n\rangle. \tag{2.8}$$

Next, we will use $\hat{O} = \hat{x}^m\hat{p}$, where $m \in \mathbb{N}$. Applying (2.1) we have

$$\begin{aligned}
0 = \langle E|\left[\frac{1}{2}\hat{p}^2 + V(\hat{x}), \hat{x}^m\hat{p}\right]|E\rangle = \langle E|\Big(\frac{1}{2}\hat{p}^2\hat{x}^m\hat{p} + V(\hat{x})\hat{x}^m\hat{p} - \\
-\frac{1}{2}\hat{x}^m\hat{p}^3 - \hat{x}^m\hat{p}V(\hat{x})\Big)|E\rangle = \langle E|\left[\frac{1}{2}\hat{x}^m\hat{p}^3 - im\hat{x}^{m-1}\hat{p}^2 - \right. \\
\left.-\frac{1}{2}m(m-1)\hat{x}^{m-2}\hat{p} + V(\hat{x})\hat{x}^m\hat{p} - \frac{1}{2}\hat{x}^m\hat{p}^3 - \hat{x}^m V(\hat{x})\hat{p} + i\hat{x}^m V'(\hat{x})\right]|E\rangle = \\
= \langle E|\left[-im\hat{x}^{m-1}\hat{p}^2 - \frac{1}{2}m(m-1)\hat{x}^{m-2}\hat{p} + i\hat{x}^m V'(\hat{x})\right]|E\rangle,
\end{aligned} \tag{2.9}$$

where $V'(\hat{x}) = \frac{\mathrm{d}V(\hat{x})}{\mathrm{d}x}$. Therefore, we get in simplified notation

$$i\langle x^m V'(x)\rangle - \frac{1}{2}m(m-1)\langle x^{m-2}p\rangle - im\langle x^{m-1}p^2\rangle = 0. \tag{2.10}$$

Substituting for $\langle x^{m-2}p\rangle$ and $\langle x^{m-1}p^2\rangle$ from (2.7) and (2.8) with $n = m-1$ we get the final recursive relation

$$2mE\langle x^{m-1}\rangle + \frac{1}{4}m(m-1)(m-2)\langle x^{m-3}\rangle - \langle x^m V'(x)\rangle - 2m\langle x^{m-1}V(x)\rangle = 0. \tag{2.11}$$

Eigenstates are normalized. Therefore $\langle x^0\rangle = 1$. For $m = 1$, this equation reduces to the Virial theorem

$$E = \frac{1}{2}\langle xV'(x)\rangle + \langle V(x)\rangle. \tag{2.12}$$

The minimal set to start recursion $S = \{E, \langle x\rangle, ...\}$ is called the search space and contains energy and a few moments. Dimension of the search space is dependent on the potential $V(\hat{x})$. As was pointed out in [14], given polynomial potential, one should expect $\dim(S) \sim \deg V(\hat{x})/|G|$, where G is any discrete symmetry group of the Hamiltonian. For example ($\omega, g, h \neq 0$)

- $V(\hat{x}) = \frac{1}{2}\omega^2\hat{x}^2$; $\quad S = \{E\}$,
- $V(\hat{x}) = g\hat{x}^3$; $\quad S = \{E, \langle x\rangle, \langle x^2\rangle\}$,
- $V(\hat{x}) = g\hat{x}^2 + h\hat{x}^4$; $\quad S = \{E, \langle x^2\rangle\}$.

So far, we have not used the last of our three pillars, identity (2.3); this is about to change. Suppose we have $\hat{O} = \sum_i c_i\hat{x}^i$, $c_i \in \mathbb{C}$. Then (2.3) gives

$$0 \leq \langle O^\dagger O\rangle = \sum_{i,j} c_i^*\langle x^{i+j}\rangle c_j = \sum_{i,j} c_i^* M_{ij} c_j, \tag{2.13}$$

where the matrix M, which elements are $M_{ij} = \langle x^{i+j} \rangle$, is called a Hankel matrix. We can see that for this form of the operator $\hat{O}$ is identity (2.3) equivalent to the statement that the symmetric matrix M is positive semi-definite. In the following algorithm, we will use a stronger constraint, which is that the matrix M should be positive definite. As we shall see, this will prove convenient.

2.2 Algorithmic structure

The main idea is to start with a large subset of the search space $X \subset S$. For each point of the subset $p = (E, \langle x \rangle, \ldots) \in X$, we generate a sequence of moments $\{\langle x^m \rangle\}_0^{2K-2}$, where K is the so-called depth of the method, with recursion relation (2.11). For this moment sequence, $K \times K$ Hankel matrix

$$M = \begin{pmatrix} \langle x^0 \rangle & \langle x^1 \rangle & \ldots & \langle x^{K-1} \rangle \\ \langle x^1 \rangle & \langle x^2 \rangle & \ldots & \langle x^K \rangle \\ \vdots & \vdots & \ddots & \vdots \\ \langle x^{K-1} \rangle & \langle x^K \rangle & \ldots & \langle x^{2K-2} \rangle \end{pmatrix} \tag{2.14}$$

is created, and its positivity is checked. If it fails the test, then the point p is dismissed. This way, we obtain a truncated set of points $X_K \subseteq X$ at depth K. This process can be done once for high depth if the allowed set of points is small enough to deduce something from the allowed set of points X_K. Another possibility is to apply this procedure subsequently on allowed regions for higher depths. Let us summarize this algorithm in a few steps.

1. Select a subset of the search space $X \subset S$. For each point $p = (E, \langle x \rangle, \ldots) \in X$ generate the moment sequence $\{\langle x^m \rangle\}_0^{2K-2}$.

2. From $2K - 2$ terms of this sequence for the point p construct the $K \times K$ Hankel matrix $M_{ij} = \langle x^{i+j} \rangle$, $0 \leq i, j \leq K - 1$.

3. Check if the matrix M is positive definite. If it is not positive definite, then dismiss the point p. This way, we obtain the set of allowed points $X_K \subseteq X$ at depth K.

4. Repeat this procedure starting with the set of points X_K and depth $K + 1$.

The expectation is that as $K \to \infty$, the allowed set of points X_K converges to values from which true spectrum can be obtained. The steps of the above algorithm are of polynomial complexity in the depth K, but convergence in K has an exponential tendency, as we will see in the case of the harmonic oscillator and the double-well potential in the next chapter. One of the method's drawbacks is that elements of the matrix M generally grow very rapidly. This growth can be dampened by rescaling matrix elements

$$M_{ij} \longrightarrow \frac{M_{ij}}{M_{i1} M_{j1}}, \tag{2.15}$$

for $M_{i1}, M_{j1} \neq 0$. This way, the signs of the principal minors are unchanged, and positive definiteness is conserved. Let us prove this little trick. From Sylvester's

criterion, we know that for a symmetric, positive definite matrix $A \in \mathbb{R}^{n\times n}$, all principal minors are positive. We can write the k-th principal minor of matrix A for $k \in \{1, \ldots, n-1\}$ using the definition of determinant of an $n \times n$ matrix

$$\det A_k = \sum_{\pi \in S_n} \operatorname{sgn}(\pi) a_{0\pi(0)} a_{1\pi(1)} \ldots a_{n-1\pi(n-1)}, \tag{2.16}$$

where S_n is the group of all permutations of the set $\{0, 1, \ldots, n-1\}$ with the function composition as group operation, π is a permutation, $\operatorname{sgn}(\pi)$ sign of the permutation and small letters denote elements of the matrix. Now we will perform (2.15) on the principal minor above

$$\det A_k \longrightarrow \sum_{\pi \in S_n} \operatorname{sgn}(\pi) \frac{a_{0\pi(0)}}{a_{01} a_{\pi(0)1}} \frac{a_{1\pi(1)}}{a_{11} a_{\pi(1)1}} \ldots \frac{a_{n-1\pi(n-1)}}{a_{n-11} a_{\pi(n-1)1}}. \tag{2.17}$$

The denominator of each member of the sum is a square. Therefore, the sign of the principal minor is unchanged.

Because of this growth, high numerical precision is needed. We worked in Python with the mpmath library. Precision was set to 50 digits as was done in [14]. Check of the positivity of the matrix M was done by trying the Cholesky decomposition on the matrix M – given symmetric, positive definite matrix M, we can write $M = LL^\top$ where L is a real lower triangular matrix with positive diagonal entries. If the Cholesky decomposition of the matrix M is not possible, it means M is not positive definite and, the moment sequence creating the matrix M is rejected. As mentioned in [14], one could try to find the singular Hankel matrices corresponding to boundary points of the accepted regions. This could speed up computations. Unfortunately, we did not find a way to isolate such matrices; thus, we opted to check positiveness using the Cholesky decomposition.

2.3 Matrix models

We will briefly outline that the bootstrapping method can also be generalized to single-matrix quantum mechanics. Firstly, we will explain what single-matrix quantum mechanics is. Quantum mechanics can be thought of as a special case of Quantum Field Theory (QFT). In QFT, we have "input space", called spacetime, and "output space", called target space. Quantum mechanics is QFT with the spacetime of one dimension, where the only dimension is time. The target space of the quantum mechanics we are used to is $\mathbb{R}^N$ (most often $N = 3$, think of position vector $\vec{x}(t)$). Single-matrix quantum mechanics works with the target space of Hermitian $N \times N$ matrices. Generally, QFTs with this type of target space are called matrix models. It is common to work in so-called large N limit, where $N \to \infty$ and certain aspects of matrix models simplify dramatically.

The Hamiltonian in this matrix model can, e.g., look like this

$$\hat{H} = \operatorname{Tr}(\hat{P}^2) + \operatorname{Tr}(\hat{X}^2) + \frac{g}{N} \operatorname{Tr}(\hat{X}^4), \tag{2.18}$$

where $\hat{P}$ and $\hat{X}$ are $N \times N$ Hermitian matrices analogous to momentum and position operator and $g > 0$ the coupling constant. Matrices $\hat{P}$ and $\hat{X}$ satisfy

commutation relations $[\hat{P}_{ij}, \hat{X}_{kl}] = -i\delta_{il}\delta_{jk}$ (where we still have $\hbar = 1$). The main difference in the bootstrap method for single-matrix quantum mechanics is that we cannot eliminate momentum operator $\hat{P}$ explicitly and isolate energy, and we do not use closed recursion relation for all expectation values. However, the energy and expectation values of short operators (operators of power less than N) can still be constrained. This time, we will need more than three basic identities; we will need to use more symmetries and tricks as large N factorization to get additional relations between expectation values. The description of these methods is beyond the range of this thesis and can be found in [1], [16] and [17].

3. Applications

The last chapter will be about applying the bootstrap method to two quantum mechanical systems – the harmonic oscillator and the double-well. The harmonic oscillator represents the simplest system to test the bootstrap method because it has only one-dimensional search space, and the results gained can be easily compared to its well-known spectrum. After that, we will move on to the double-well, which has two-dimensional search space. Therefore, it will pose new challenges. We will compare the results gained with the methods described in the first chapter. In both cases, we will go through the intricacies of implementing the bootstrap in Python.

3.1 Harmonic Oscillator

We will work with a particle in the harmonic oscillator potential

$$V(\hat{x}) = \frac{1}{2}\hat{x}^2, \tag{3.1}$$

where frequency of oscillations ω, mass of the particle M and Planck's reduced constant $\hbar$ are all set to one as we did before. Using the recursive relation for expectation values (2.11) we get

$$\begin{aligned} 0 &= 2mE\langle x^{m-1}\rangle + \frac{1}{4}m(m-1)(m-2)\langle x^{m-3}\rangle - \langle x^m V'(x)\rangle - 2m\langle x^{m-1}V(x)\rangle = \\ &= 2mE\langle x^{m-1}\rangle + \frac{1}{4}m(m-1)(m-2)\langle x^{m-3}\rangle - \langle x^{m+1}\rangle - m\langle x^{m+1}\rangle, \end{aligned} \tag{3.2}$$

and after substitution $m = s - 1$ where $m \in \mathbb{N}$, therefore $s \in \{2, 3, 4, \ldots\}$ we get the recursion relation for the harmonic oscillator

$$s\langle x^s\rangle = 2E(s-1)\langle x^{s-2}\rangle + \frac{1}{4}(s-1)(s-2)(s-3)\langle x^{s-4}\rangle. \tag{3.3}$$

This way, we have the recursion relation only for even moments. However, the potential $V(x)$ is even, which means that all odd moments are equal to zero. From normalization, we know that $\langle x^0\rangle = 1$, and from equation (3.3), we see that $\langle x^2\rangle = E$ and this is all we need to start the recursion. Thus, the search space is truly one-dimensional $S = \{E\}$.

Now, we will proceed to implementation details. Figure 3.2 presents the program we will go through. We started with importing libraries; we used `scipy` and `numpy` for fitting data, `matplotlib.pyplot` for plotting, and most importantly, `mpmath` for the high precision. By a command `mp.dps`, the precision for the real float type `mpf`, with which we worked, was set to 50 digits. In order to maintain high precision, we used special arithmetic operations from `mpmath` library – `fadd` for addition, `fsub` for subtraction, `fmul` and `fprod` for multiplication, `fdiv` for division and `power` for exponentiation.

Then we moved on to defining some functions. The `MakingGrid` function created a high-precision one-dimensional grid, and we used it to divide the interval of energies from $E_{\min} = 0$ to $E_{\max} = 10$ to $N = 1000$ pieces. The `RecursionRelation` function produced a moment sequence $\{\langle x^s \rangle\}_0^{2K-2}$ according to equation (3.3). From this sequence, the function `HankelMatrix` created a $K \times K$ Hankel matrix where we also used the trick (2.15) to dampen the growth of matrix elements. The last function `fitting_function` was used for fitting gained data; we will comment on that later.

After that, we initialized parameters and variables and created the search space S. Consequently, we started the primary cycle, reducing the search space until $K > 50$. For every energy from the search space, we created a moment sequence, and from that, the Hankel matrix. Positivity was checked by trying the Cholesky decomposition by the function `cholesky`. If it failed, we replaced the relevant energy by 0. This way, we obtained the reduced search space. Then we went through it to find the boundaries for the accepted regions of energies, creating a list `bounds1`. This list was checked for duplicated values. If there was a duplicated value, it meant that the relevant region of the accepted energies was only one value. Therefore, this value was transferred into `results` list together with a current size of a step as uncertainty to this value, as a potential member of the spectrum. Either it was a member of the spectrum to which the algorithm correctly converged or one of the accepted regions "crumbled" — it did not simply shrink; instead, one part of it was riddled with holes in such a way that the one-value accepted regions existed. We will comment on this issue later. This way, we created a modified list of boundaries called `bounds2`. From this list, we calculated the total width of the accepted energy intervals for given K and saved it in the `convergence` list to study the convergence of the method.

Most importantly, from the modified list of boundaries, we created new grids for the accepted regions only and applied the whole process again to these accepted regions. After depth $K = 50$ was reached, we took the average from the last boundaries for each region and saved it in the `results` list together with the half-length of each region as uncertainty to the averaged value. This way, we obtained the accepted energies with their uncertainties, which are compared with the exact spectrum of the harmonic oscillator in Table 3.1.

Firstly, we can see no impostors in the accepted energies caused by the "crumbling" mentioned earlier, and the bootstrapped results are in good agreement with the exact spectrum. Secondly, we can see that the relative difference from the exact value is more significant for higher energies. This also holds for the uncertainties, except for the first bootstrapped energy. The first energy was isolated to the one-value region for $K = 10$; therefore, it has the uncertainty of the initial step size. The other bootstrapped energies were not isolated to one-value regions; instead, they were averaged from the last regions, which were wider for higher energies. This effect was also observed with the double-well potential, as we will see later.

n	E_n	Bootstrapped energy	Relative difference from the exact value
0	1/2	0.50 ± 0.01	$1.2 \cdot 10^{-50}$
1	3/2	$1.499999999999999996 \pm 9 \cdot 10^{-18}$	$2.8 \cdot 10^{-18}$
2	5/2	$2.500000000000001 \pm 3 \cdot 10^{-15}$	$4.6 \cdot 10^{-16}$
3	7/2	$3.4999999999998 \pm 4 \cdot 10^{-13}$	$5.4 \cdot 10^{-14}$
4	9/2	$4.50000000001 \pm 3 \cdot 10^{-11}$	$2.9 \cdot 10^{-12}$
5	11/2	$5.499999999 \pm 1 \cdot 10^{-9}$	$1.0 \cdot 10^{-10}$
6	13/2	$6.50000001 \pm 4 \cdot 10^{-8}$	$1.8 \cdot 10^{-9}$
7	15/2	$7.500000 \pm 1 \cdot 10^{-6}$	$5.5 \cdot 10^{-8}$
8	17/2	$8.50001 \pm 2 \cdot 10^{-5}$	$6.5 \cdot 10^{-7}$
9	19/2	$9.4999 \pm 2 \cdot 10^{-4}$	$6.9 \cdot 10^{-6}$

Table 3.1: Comparison of the bootstrapped energies with the exact spectrum of the harmonic oscilator $E_n = n + 1/2$ (in units of $\hbar\omega$).

In the last part of the program, we used data saved in `convergence` list to not only create in `matplotlib.pyplot` library a graph of convergence of the method in Figure 3.1 but also to fit the data using orthogonal distance regression `odr` from `scipy` library. As a fitting function, we used

$$y = ae^{-b(K-10)^c}, \tag{3.4}$$

where y is the total interval width and a, b and c are fitted real parameters. We obtained $a = 8.0 \pm 0.3$, $b = 0.004 \pm 0.002$, and $c = 1.9 \pm 0.2$. Thus, convergence is faster than exponential.

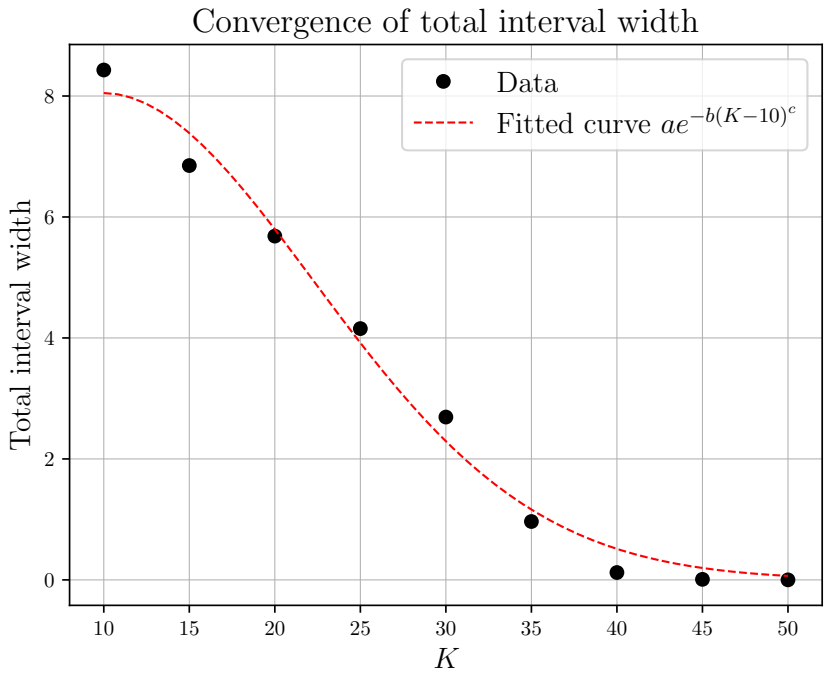

Figure 3.1: Convergence of the method for the harmonic oscillator.

We have also created another less complicated and faster program in which we applied the algorithm only once for $K = 50$ and $N = 10\,000$. This time, all accepted energies were reduced to one-value regions; therefore, they had the same

uncertainty of the initial step size 0.001. Both approaches agreed in results, but the subsequent one represented in Figure 3.2 was less stable in the choice of parameters K and N. This means that for some values of these parameters, the correct energy was discarded because the depth K was too high for the fineness of a grid of the relevant region. Therefore, parameters K and N had to be carefully chosen based on trial and error. Also, individual approaches cannot differentiate between the impostor value and the correct value. We used both and compared the results to discard the incorrect values (there were none this time). The following section will discuss other benefits of using both approaches and their comparison. Both programs are included in the attachments to this thesis.

```
import numpy as np
import scipy as sp
from scipy import odr
import matplotlib.pyplot as plt
from mpmath import *
mp.dps = 50
plt.rcParams.update({
    "text.usetex": True,
    "font.family": "cmr"
})

#making the grid
def MakingGrid(start,end,arr,step):
  x = start
  while x <= end:
    arr.append(x)
    x = fadd(x,step)
  return(arr)

#recursion for creating the moment sequence
def RecursionRelation(y,x,K):
  x =[1,0,mpf(y),0]
  for s in range(4,2*K-1):
    if s%2 == 0:
      x.append(fadd(fdiv(fprod([2,y,(s-1),x[s-2]]),s),
      fdiv(fprod([s-1,s-2,s-3,x[s-4]]),fmul(4,s))))
    else:
      x.append(0)
  return x

#creating the Hankel matrix from the moment sequence
def HankelMatrix(x):
  d = int((len(x) + 1)/2)
  H = zeros(d)
  for i in range(0,d):
    for j in range(0,d):
      if fmul(x[i+1],x[j+1]) != 0:
        H[i,j] = fdiv(x[i+j],fmul(x[i+1],x[j+1]))
      else:
        H[i,j] = x[i+j]
  return H

#defining the fitting function
```

```
def fitting_function(p,x):
  a,b,c = p
  return a*np.exp(-b*(x-10)**c)

#creating the search space
N = power(10,3)
K = 10
K_list = []
E_min, E_max = 0, 10
length = fsub(E_max,E_min)
S = [MakingGrid(E_min,E_max,[],fdiv(length,N))]
S_reduced = [MakingGrid(E_min,E_max,[],fdiv(length,N))]
results = []
convergence = []

while K<=50:
  #reducing the search space
  for j in range(0,len(S)):
    for i in range(0,len(S[j])):
      O = RecursionRelation(S[j][i],[],K)
      try:
        M = HankelMatrix(O)
        L = cholesky(M)
      except ValueError:
        S_reduced[j][i] = 0
  print(f"\n Reduced search space for K = {K}: \n",S_reduced)

  bounds1 = []
  for j in range(0,len(S_reduced)):
    for i in range(1,len(S_reduced[j])-1):
      if i==1 and S_reduced[j][0]!=0:
        bounds1.append(S_reduced[j][0])
      if i==len(S_reduced[j])-2 and S_reduced[j][-1]!=0:
        bounds1.append(S_reduced[j][-1])
      if ((S_reduced[j][i-1]==0) and (S_reduced[j][i]!=0)):
        bounds1.append(S_reduced[j][i])
      if ((S_reduced[j][i+1]==0) and (S_reduced[j][i]!=0)):
        bounds1.append(S_reduced[j][i])
      if ((S_reduced[j][i-1]==0) and (S_reduced[j][i]!=0) and
      (S_reduced[j][i+1]==0)):
        results.append([S_reduced[j][i],fdiv(fsub(S[j][i+1],S[j][
   i-1]),2)])
  print(f"\n Bounds for accepted regions for K = {K}: \n",bounds1
   )

  bounds2 = []
  for i in range(0,len(bounds1)-1,2):
    if bounds1[i] != bounds1[i+1]:
      bounds2.append(bounds1[i])
      bounds2.append(bounds1[i+1])
  print(f"\n Modified bounds for accepted regions for K = {K}: \n
   ",bounds2)

  totwidth = 0
  if len(bounds2)>=2:
    for i in range(0,len(bounds2)-1,2):
      totwidth = fadd(totwidth,fsub(bounds2[i+1],bounds2[i]))
  convergence.append(totwidth)
```

```
99
100   S = []; S_reduced = []
101   for i in range(0,int(len(bounds2)/2)):
102     S.append(MakingGrid(bounds2[2*i],bounds2[2*i+1],[],
103     fdiv(fsub(bounds2[2*i+1],bounds2[2*i]),N)))
104     S_reduced.append(MakingGrid(bounds2[2*i],bounds2[2*i+1],[],
105     fdiv(fsub(bounds2[2*i+1],bounds2[2*i]),N)))
106   K_list.append(K)
107   K += 5
108
109 for i in range(0,int(len(bounds2)/2)):
110   results.append([fdiv(fadd(bounds2[2*i],bounds2[2*i+1]),2),
111   fdiv(fsub(bounds2[2*i+1],bounds2[2*i]),2)])
112 print("\n Accepted energies are: \n",results)
113 print("\n Total width of accepted energies for given K: \n",
      convergence)
114
115 #fitting data for convergence
116 for i in range(0,len(convergence)):
117   convergence[i] = float(str(convergence[i]))
118
119 odr_model = sp.odr.Model(fitting_function)
120 data = odr.Data(K_list,convergence)
121 fit = sp.odr.ODR(data,odr_model,beta0=[7,0.0001,3])
122 out = fit.run()
123 beta = out.beta
124 std = out.sd_beta
125 print("\n Parameters of the fit: ",beta,
126 "\n Standart deviation of the parameters of the fit: ",std)
127
128 #plotting
129 plt.plot(K_list,convergence,color = "black",marker = "o",
      linestyle = "None")
130 plt.plot(np.linspace(K_list[0],K_list[-1],50),
131 beta[0]*np.exp(-beta[1]*(np.linspace(K_list[0],K_list[-1],50)-10)
      **beta[2]),
132 color = "red", linestyle = "--", linewidth = 1)
133 plt.legend(["Data","Fitted curve $ae^{-b(K-10)^c}$"],loc = "upper
      right", fontsize=14)
134 plt.title("Convergence of total interval width",fontsize=16)
135 plt.xlabel("$K$",fontsize=14)
136 plt.ylabel("Total interval width",fontsize=14)
137 plt.grid(linestyle = '-', linewidth = 0.5)
138 plt.savefig("ConvergenceHO.pdf", dpi=300)
```

Figure 3.2: Implementation of the bootstrap method for the harmonic oscillator in Python.

3.2 Double-Well

We will work with a particle in the double-well potential

$$V(\hat{x}) = \frac{g}{2}\left(\hat{x}^2 - \frac{1}{4g}\right)^2, \; g > 0. \tag{3.5}$$

Using the recursive relation for expectation values (2.11) we get

$$
\begin{aligned}
0 &= 2mE\langle x^{m-1}\rangle + \frac{1}{4}m(m-1)(m-2)\langle x^{m-3}\rangle - \langle x^m V'(x)\rangle - 2m\langle x^{m-1}V(x)\rangle = \\
&= 2mE\langle x^{m-1}\rangle + \frac{1}{4}m(m-1)(m-2)\langle x^{m-3}\rangle - \left\langle 2gx^{m+3} - \frac{1}{2}x^{m+1}\right\rangle - \\
&- 2m\left\langle x^{m-1}\frac{g}{2}\left(x^4 - \frac{1}{2g}x^2 + \frac{1}{16g^2}\right)\right\rangle = \left(2E - \frac{1}{16g}\right)m\langle x^{m-1}\rangle + \\
&+ \frac{1}{4}m(m-1)(m-2)\langle x^{m-3}\rangle + \frac{1}{2}(m+1)\langle x^{m+1}\rangle - g(m+2)\langle x^{m+3}\rangle, \qquad (3.6)
\end{aligned}
$$

and after substitution $m = s - 3$ where $m \in \mathbb{N}$, therefore $s \in \{4, 5, 6, \ldots\}$ we get the recursion relation for the double-well potential

$$
\begin{aligned}
\langle x^s\rangle = \frac{1}{2g}\frac{s-2}{s-1}\langle x^{s-2}\rangle + \frac{1}{g}\left(2E - \frac{1}{16g}\right)\frac{s-3}{s-1}\langle x^{s-4}\rangle + \\
+ \frac{1}{4g}\frac{(s-3)(s-4)(s-5)}{s-1}\langle x^{s-6}\rangle. \qquad (3.7)
\end{aligned}
$$

Again, we will use the evenness of the potential $V(x)$ and get that all odd moments are equal to zero. From normalization, we know that $\langle x^0\rangle = 1$, and from equation (3.7), we see that

$$
\langle x^4\rangle = \frac{1}{3g}\left(2E - \frac{1}{16g}\right) + \frac{1}{3g}\langle x^2\rangle, \qquad (3.8)
$$

where E and $\langle x^2\rangle$ are needed to start the recursion. Thus, the search space is two-dimensional $S = \{E, \langle x^2\rangle\}$.

Now, we will proceed to implementation details. Figure 3.8 presents the program we will go through. The core of the program – used libraries, functions, and algorithm remains the same as in the programs for the harmonic oscillator (of course, this time, we use the recursive relation (3.7) in `RecursionRelation` function). The first new challenge was to estimate the relevant interval of the second moment, given the interval of the energy. We used a classical particle in the double-well potential (as was done in [15]). For a period of motion of getting from turning point x_1 to turning point x_2 and back, we have

$$
T = 2\int_{x_1}^{x_2} \frac{\mathrm{d}x}{\sqrt{2E - g\left(x^2 - \frac{1}{4g}\right)^2}}, \qquad (3.9)
$$

and for the second moment

$$
\langle x^2\rangle_{\mathrm{cl}} = \frac{2}{T}\int_{x_1}^{x_2} \frac{x^2}{\sqrt{2E - g\left(x^2 - \frac{1}{4g}\right)^2}}\,\mathrm{d}x. \qquad (3.10)
$$

This curve represents the classical limit in the E-$\langle x^2\rangle$ plane, our search space S. Because of that, the accepted regions by the bootstrap method have to be close

to this curve, as is depicted in Figure 3.4 and Figure 3.5. In the program, we used equations (3.9) and (3.10) to estimate the interval of the second moment. The second challenge was to create and reduce a two-dimensional grid. We created one one-dimensional grid for energies and, for each energy, another one-dimensional grid for second moments, all grids with $N = 300$. For each energy and grid of second moments related to that energy, the moment sequence $\{\langle x^s \rangle\}_0^{2K-2}$ and consequently $K \times K$ Hankel matrix was created, and its positive definiteness checked by trying the Cholesky decomposition. If the whole one-dimensional grid for second moments for a given energy was rejected, then the energy was replaced by 0. We were left with a reduced one-dimensional search space of energies on which we applied the same procedure as for the harmonic oscillator to get the boundaries for the accepted energies.

Again, we calculated the total width of the accepted energy intervals for given K and saved it in the `convergence` list to study the convergence of the method. New grids for the accepted regions of energies were made, and the process was repeated. After depth $K = 18$ was reached, we took the average from the last boundaries for each region and saved it in the `results` list. This way, we obtained the accepted energies presented in Table 3.2. Some of the values proved to be the impostors discussed in the last section, and we discarded them because of Figure 3.4 and Figure 3.5 (we will discuss these figures and finding the impostors later). This time, there was not so great difference in uncertainties of individual energies as was the case for the harmonic oscillator, but still higher energies were less constrained; also, it can be seen from Figure 3.4 and Figure 3.5.

Bootstrapped energy at $g = 0.05$		
$0.3850 \pm 4 \cdot 10^{-4}$	~~$1.846 \pm 3 \cdot 10^{-3}$~~	$2.8316 \pm 4 \cdot 10^{-4}$
$0.4600 \pm 7 \cdot 10^{-4}$	~~$1.884 \pm 3 \cdot 10^{-3}$~~	$2.8556 \pm 5 \cdot 10^{-4}$
$0.4971 \pm 2 \cdot 10^{-4}$	$2.244 \pm 2 \cdot 10^{-3}$	$2.8798 \pm 6 \cdot 10^{-4}$
$1.0643 \pm 8 \cdot 10^{-4}$	$2.263 \pm 2 \cdot 10^{-3}$	$2.9040 \pm 6 \cdot 10^{-4}$
$1.598 \pm 3 \cdot 10^{-3}$	$2.283 \pm 2 \cdot 10^{-3}$	$2.9284 \pm 7 \cdot 10^{-4}$
~~$1.808 \pm 3 \cdot 10^{-3}$~~	$2.784123 \pm 9 \cdot 10^{-6}$	$2.9530 \pm 7 \cdot 10^{-4}$
~~$1.829 \pm 3 \cdot 10^{-3}$~~	$2.8078 \pm 2 \cdot 10^{-4}$	$2.9777 \pm 6 \cdot 10^{-4}$

Table 3.2: The bootstrapped energies for the double-well potential obtained by subsequently applying the bootstrap method (in units of $\hbar\omega$). Red ones are the impostors discarded by Figure 3.4 and Figure 3.5.

In the last part of the program, we used data saved in `convergence` list to not only create in `matplotlib.pyplot` library a graph of convergence of the method in Figure 3.3 but also to fit the data using orthogonal distance regression `odr` from `scipy` library. We used (3.4) as the fitting function, where a, b and c are fitted real parameters. We obtained $a = 2.37 \pm 0.08$, $b = 0.04 \pm 0.02$, and $c = 2.2 \pm 0.2$. Thus, convergence is again faster than exponential.

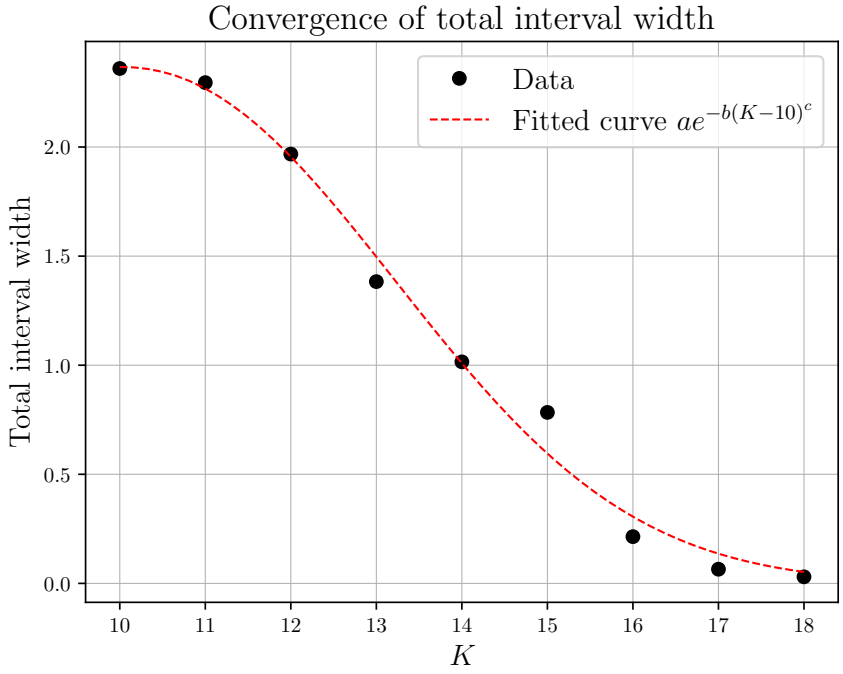

Figure 3.3: Convergence of the method for the double-well.

We have also created another less complicated and faster program in which we applied the algorithm only once for $K = 16$ and $N = 600$. In this program, we did not focus on energies only but created Figure 3.4, where accepted regions of the search space are depicted together with the curve for the classical particle. For creating this picture, it was more convenient to construct the search space oppositely – only one one-dimensional grid for second moments and a one-dimensional grid of energies for each second moment. Also, from the data obtained from the discussed program in Figure 3.8, we made another program which created Figure 3.5, where the reduction of the subsequent approach and the curve for the classical particle is depicted.

These figures are significant because the program in Figure 3.8 cannot differentiate between the impostor value and the correct value on its own; however, the correct value would be depicted in these figures. We can see that the discarded energies from Table 3.2 have no region in Figure 3.4, and they have no darkest region in Figure 3.5. Comparing these figures, we can see that the one-run approach and subsequent approach agree well about the accepted regions, and we did not miss any regions with the one-run method. The subsequent method is again less stable in the choice of parameters K and N, as was discussed in the last section. On the other hand, the subsequent approach is better when one tries the method on a system without prior knowledge. One can easily spot that some regions were incorrectly rejected. We recommend using the subsequent approach to get to know the new system and then using the one-run approach with calibrated parameters K and N in more complicated programs.

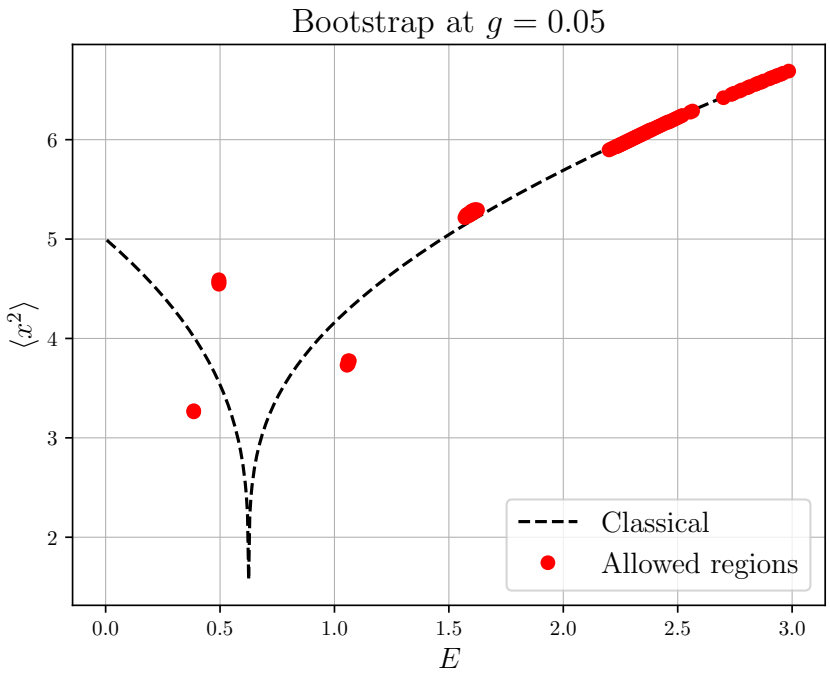

Figure 3.4: Reduced search space after one run of the bootstrap method for $K = 16$ and $N = 600$ together with the curve for the classical particle.

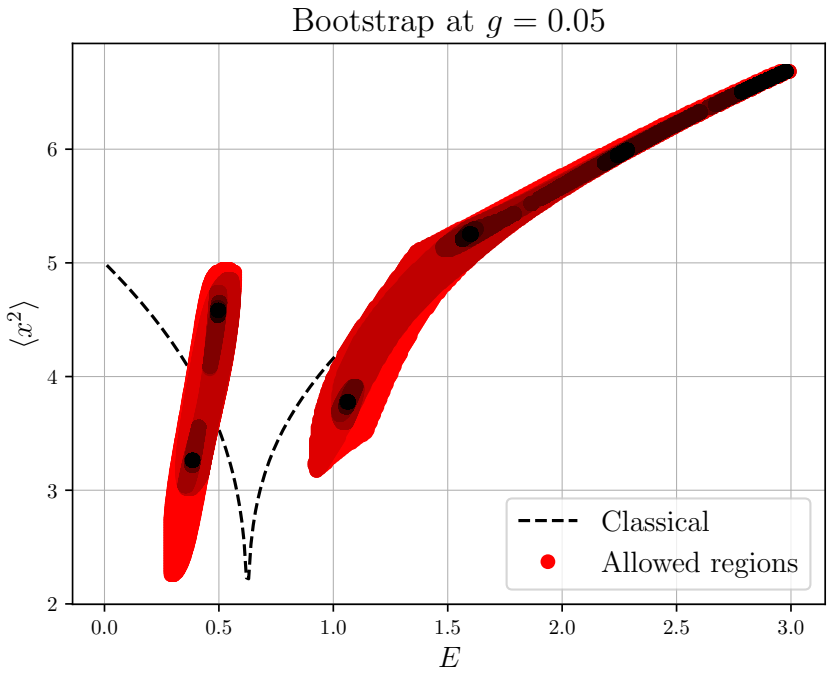

Figure 3.5: Reduced search space after subsequently running the bootstrap method for K from 10 (lightest) to 18 (darkest) and $N = 300$ together with the curve for the classical particle.

And that is precisely what we did in the two more programs where we focused on the ground and the first excited states. We repeated the one-run approach for different values of the coupling constant g (from 0.037 to 0.050 with a step

of 0.001) to get the dependence of ground state and first excited state energy on g in Figure 3.6 and also the dependence of energy difference of these two energies on g in Figure 3.7 (in both programs we used $K = 18$ and $N = 900$).

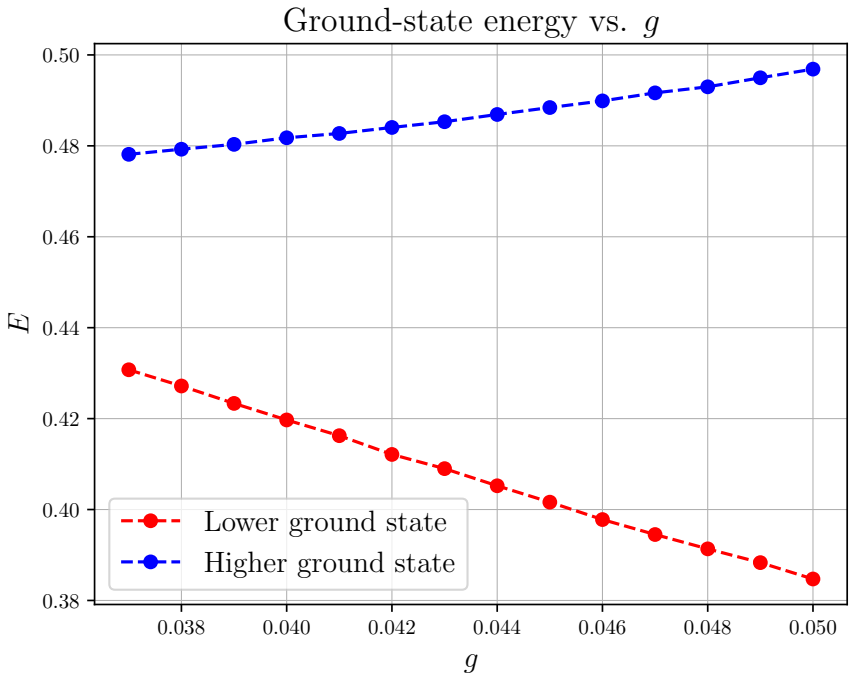

Figure 3.6: Dependence of energies of the ground and the first excited state on the coupling constant g. Both energies are closing on each other as $g \to 0$.

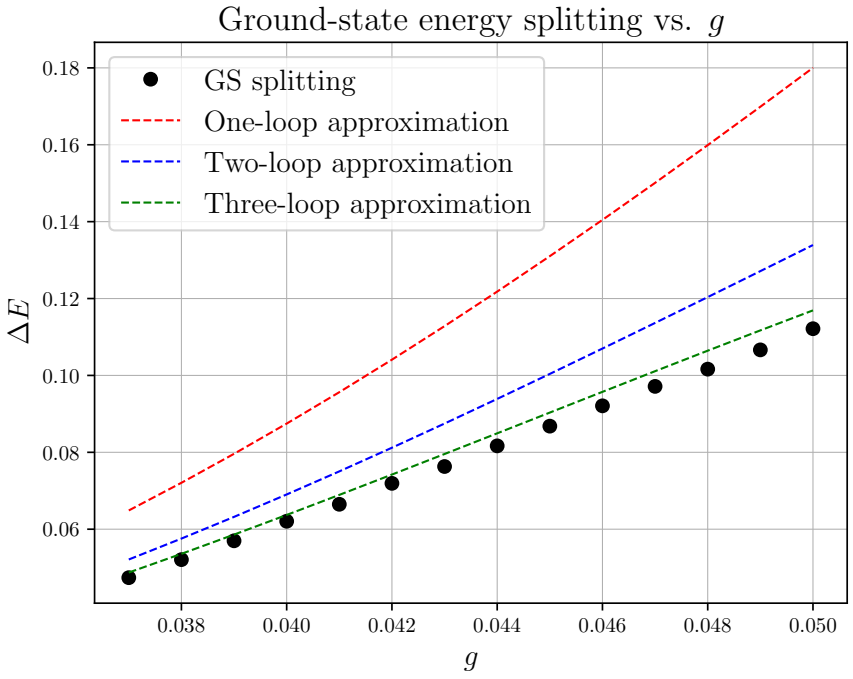

Figure 3.7: Dependence of energy difference of the ground and the first excited state on the coupling constant g in comparison with the one-loop (equivalent with the WKB), the two-loop, and the three-loop approximation method.

From Figure 3.6, we can see that both energies are closing on each other as they should in the $g \to 0$ limit when the double-well becomes two single-wells. Also, from Figure 3.7, we can see that the bootstrap method is better than the one-loop (which is equivalent to the WKB) and the two-loop approximation, and it is in good agreement with the three-loop on the used interval of g. All approximations are closing on the bootstrapped data in the $g \to 0$ limit. All programs are included in the attachments to this thesis.

```
import numpy as np
import scipy as sp
from scipy import odr
import matplotlib.pyplot as plt
from mpmath import *
mp.dps = 50
plt.rcParams.update({
    "text.usetex": True,
    "font.family": "cmr"
})

#making the grid
def MakingGrid(start,end,arr,step):
  x = start
  while x <= end:
    arr.append(x)
    x = fadd(x,step)
  return(arr)

#recursion for creating the moment sequence
def RecursionRelation(x,y,z,w,K):
  x =[1,0,mpf(z),0,fdiv(fadd(fsub(fmul(2,mpf(y)),fdiv(1,fmul(16,
   mpf(w)))),mpf(z)),
  fmul(3,mpf(w))),0]
  for s in range(6,2*K-1):
    if s%2 == 0:
      x.append(fsum([fdiv(fprod([fsub(fmul(2,mpf(y)),fdiv(1,fmul
   (16,mpf(w)))),
      s-3,x[s-4]]),fmul(mpf(w),(s-1))),fdiv(fmul(s-2,x[s-2]),
   fprod([2,mpf(w),s-1])),
      fdiv(fprod([s-3,s-4,s-5,x[s-6]]),fprod([4,mpf(w),(s-1)]))])
   )
    else:
      x.append(0)
  return x

#creating the Hankel matrix from the moment sequence
def HankelMatrix(x):
  d = int((len(x) + 1)/2)
  H = zeros(d)
  for i in range(0,d):
    for j in range(0,d):
      if fmul(x[i+1],x[j+1]) != 0:
        H[i,j] = fdiv(x[i+j],fmul(x[i+1],x[j+1]))
      else:
        H[i,j] = x[i+j]
  return H

```

```
#defining the fitting function
def fitting_function(p,x):
  a,b,c = p
  return a*np.exp(-b*(x-10)**c)

#creating the search space
g = 0.05
N = 300
K = 10; K_max = 18
K_list = []
E_min, E_max = 0, 3
if E_max<=(1/(32*g)):
  x1 = sqrt((1/(2*g)-sqrt(8*E_max/g))/2)
  x2 = sqrt((1/(2*g)+sqrt(8*E_max/g))/2)
else:
  x1 = -sqrt((1/(2*g)+sqrt(8*E_max/g))/2)
  x2 = sqrt((1/(2*g)+sqrt(8*E_max/g))/2)
integrand1 = lambda x: 1/(sqrt(2*E_max-g*(x**2-1/(4*g))**2))
integrand2 = lambda x: x**2/(sqrt(2*E_max-g*(x**2-1/(4*g))**2))
T = 2*re(quad(integrand1,[x1,x2]))
mom_max = 2*re(quad(integrand2,[x1,x2])/T); mom_min = 0

length1 = fsub(E_max,E_min)
length2 = fsub(mom_max,mom_min)
S1 = [MakingGrid(E_min,E_max,[],fdiv(length1,N))]
S2 = MakingGrid(mom_min,mom_max,[],fdiv(length2,N))
S1_reduced = [MakingGrid(E_min,E_max,[],fdiv(length1,N))]
S2_reduced = MakingGrid(mom_min,mom_max,[],fdiv(length2,N))
results = []
convergence = []

while K<=K_max:
  #reducing the search space
  for k in range(0,len(S1)):
    for i in range(0,len(S1[k])):
      for j in range(0,len(S2)):
        O = RecursionRelation([],S1[k][i],S2[j],g,K)
        try:
          M = HankelMatrix(O)
          L = cholesky(M)
        except ValueError:
          S2_reduced.remove(S2[j])
      if S2_reduced == []:
        S1_reduced[k][i] = 0
      S2_reduced = MakingGrid(mom_min,mom_max,[],fdiv(length2,N))

  print(f"\n Reduced search space for K = {K}: \n",S1_reduced)

  bounds1 = []
  for j in range(0,len(S1_reduced)):
    for i in range(1,len(S1_reduced[j])-1):
      if i==1 and S1_reduced[j][0]!=0:
        bounds1.append(S1_reduced[j][0])
      if i==len(S1_reduced[j])-2 and S1_reduced[j][-1]!=0:
        bounds1.append(S1_reduced[j][-1])
      if ((S1_reduced[j][i-1]==0) and (S1_reduced[j][i]!=0)):
        bounds1.append(S1_reduced[j][i])
      if ((S1_reduced[j][i+1]==0) and (S1_reduced[j][i]!=0)):
```

```
        bounds1.append(S1_reduced[j][i])
      if ((S1_reduced[j][i-1]==0) and (S1_reduced[j][i]!=0) and
      (S1_reduced[j][i+1]==0)):
        results.append([S1_reduced[j][i],fdiv(fsub(S1[j][i+1],S1[
    j][i-1]),2)])
  print(f"\n Bounds for accepted regions for K = {K}: \n",bounds1
    )

  bounds2 = []
  for i in range(0,len(bounds1)-1,2):
    if bounds1[i] != bounds1[i+1]:
      bounds2.append(bounds1[i])
      bounds2.append(bounds1[i+1])
  print(f"\n Modified bounds for accepted regions for K = {K}: \n
    ",bounds2)

  totwidth = 0
  if len(bounds2)>=2:
    for i in range(0,len(bounds2)-1,2):
      totwidth = fadd(totwidth,fsub(bounds2[i+1],bounds2[i]))
  convergence.append(totwidth)

  S1 = []; S1_reduced = []
  for i in range(0,int(len(bounds2)/2)):
    S1.append(MakingGrid(bounds2[2*i],bounds2[2*i+1],[],
    fdiv(fsub(bounds2[2*i+1],bounds2[2*i]),N)))
    S1_reduced.append(MakingGrid(bounds2[2*i],bounds2[2*i+1],[],
    fdiv(fsub(bounds2[2*i+1],bounds2[2*i]),N)))
  K_list.append(K)
  K += 1

for i in range(0,int(len(bounds2)/2)):
  results.append([fdiv(fadd(bounds2[2*i],bounds2[2*i+1]),2),
  fdiv(fsub(bounds2[2*i+1],bounds2[2*i]),2)])
results.sort()
print("\n Accepted energies are: \n",results)
print("\n Total width of accepted energies for given K: \n",
    convergence)

#fitting data for convergence
for i in range(0,len(convergence)):
  convergence[i] = float(str(convergence[i]))

odr_model = sp.odr.Model(fitting_function)
data = odr.Data(K_list,convergence)
fit = sp.odr.ODR(data,odr_model,beta0=[2,0.02,3])
out = fit.run()
beta = out.beta
std = out.sd_beta
print("\n Parameters of the fit: ",beta,
"\n Standart deviation of the parameters of the fit: ",std)

#plotting
plt.plot(K_list,convergence,color = "black",marker = "o",
    linestyle = "None")
plt.plot(np.linspace(K_list[0],K_list[-1],50),
beta[0]*np.exp(-beta[1]*(np.linspace(K_list[0],K_list[-1],50)-10)
    **beta[2]),
```

```
color = "red", linestyle = "--", linewidth = 1)
plt.legend(["Data","Fitted curve $ae^{-b(K-10)^c}$"],loc = "upper
    right", fontsize=14)
plt.title("Convergence of total interval width",fontsize=16)
plt.xlabel("$K$",fontsize=14)
plt.ylabel("Total interval width",fontsize=14)
plt.grid(linestyle = '-', linewidth = 0.5)
plt.savefig("ConvergenceDoubleWell.pdf", dpi=300)
```

Figure 3.8: Implementation of the bootstrap method for the double-well in Python.

Conclusion

We introduced the bootstrap method in quantum mechanics and implemented it in Python to attack two simple systems – the harmonic oscillator and the double-well. We found out that bootstrapped energies agreed with the exact spectrum for the harmonic oscillator. For the double-well potential, we found out that the bootstrapped energies agreed with the classical limit, and we focused on the ground-state energy splitting.

To better understand and compare the ground-state energy splitting with the numerical bootstrap, we investigated two different analytical approaches – the WKB approximation and the path integral around instanton (the one-loop approximation), which proved to be equivalent. We found out that the bootstrap method outperformed these two approximations. We reached for better approximations – the two-loop and the three-loop approximation. We found that the bootstrap method gave a better estimate than the two-loop approximation and agreed well with the three-loop approximation.

We went through the details of our implementation in Python. We explored two approaches to the bootstrap method – the one-run and the subsequent approach. We found that the one-run approach is faster and more stable than the subsequent one and, therefore, more suitable for more complicated programs. However, in systems with no prior knowledge, it is more convenient to use the subsequent approach because it is easier to spot that we missed some energies. We recommend using the subsequent approach to get to know the new system and then using the one-run approach with calibrated parameters in more complicated programs.

To conclude, for both systems, the bootstrap method proved successful. It gave us a great estimate of the spectrum for both systems. In the case of the double-well, it even gave us better results than the standard approximation methods.

References

[1] X. Han, S.A. Hartnoll, and J. Kruthoff. Bootstrapping Matrix Quantum Mechanics. Phys. Rev. Lett., 125(041601), 2020. doi:10.1103/PhysRevLett.125.041601. arXiv:2004.10212 [hep-th].

[2] B. Zwiebach. Mastering quantum mechanics: Essentials, Theory, and Applications. First edition. The MIT Press, Cambridge, Massachusetts, 2022. ISBN 9780262366892.

[3] P. Cejnar. A Condensed Course of Quantum Mechanics. First edition. Karolinum Press, Prague, 2013. ISBN 9788024623214.

[4] J. Novotný. Vybrané partie z teorie kvantovaných polí. `https://www-ucjf.troja.mff.cuni.cz/~novotny/text23.pdf`, 1999. Accessed: 2024-6-12.

[5] M. Marino. Instantons and Large N: An Introduction to Non-Perturbative Methods in Quantum Field Theory. First edition. Cambridge University Press, Cambridge, United Kingdom, 2015. ISBN 9781316365540.

[6] H. Kleinert. Path Integrals in Quantum Mechanics, Statistics, Polymer Physics, and Financial Markets. Fifth edition. World Scientific Publishing Company, Berlin, 2009. ISBN 9814273562.

[7] J. Glimm and A. Jaffe. Quantum Physics: A Functional Integral Point of View. Second edition. Springer-Verlag, New York, Heidelberg, Berlin, 1987. ISBN 0387964770.

[8] M.J. Ablowitz and A.S. Fokas. Complex Variables. Second edition. Cambridge University Press, Cambridge, United Kingdom, 2003. ISBN 9780521534291.

[9] C.M. Bender and S.A. Orszag. Advanced Mathematical Methods for Scientists and Engineers. Second edition. Springer, United States of America, 1999. ISBN 9780387989310.

[10] R. Černý and M. Pokorný. Základy matematické analýzy pro studenty fyziky 4. First edition. MatfyzPress, Prague, 2024. ISBN 9788073785093.

[11] M. Moriconi. Nodes of wavefunctions. arXiv:quant-ph/0702260, 2007. Accessed: 2024-16-12.

[12] J. Zinn-Justin. Quantum Field Theory and Critical Phenomena. Fifth edition. Oxford University Press, Oxford, United Kingdom, 2021. ISBN 9780198834625.

[13] M.A. Escobar-Ruiz, E. Shuryak, and A.V. Turbiner. Three-loop Corection to the Instanton Density for the Double Well Potential. Phys. Rev. D, 92 (025046), 2015. doi:10.1103/PhysRevD.92.025046.

[14] D. Bernstein and G. Hulsey. Bootstrapping Simple QM Systems. arXiv:2108.08757 [hep-th], 2021. Accessed: 2024-6-12.

[15] D. Bernstein and G. Hulsey. Bootstrapping more QM systems. Journal of Physics A: Mathematical and Theoretical, 55(27), 2022. doi:10.1088/1751-8121/ac7118. arXiv:2109.06251 [hep-th].

[16] M. Marino. Chern–Simons theory, matrix models and topological strings. First edition. Cambridge University Press, Cambridge, United Kingdom, 2005. ISBN 9780198568490.

[17] D. Anninos and Mühlmann B. Notes on Matrix Models. arXiv:2004.01171 [hep-th], 2020. Accessed: 2024-6-12.